Biochemical and chemical biological approaches to mammalian sleep: roles of calcineurin in site-specific dephosphorylation and sleep regulation

Jianjun Yu[1,2,*], Tao V. Wang[1,2,*], Rui Gao[1,*], Chenggang Li[2,3,*], Huijie Liu[2,3,*], Lu Yang[1,2], Yuxiang Liu[1,2,3], Yunfeng Cui[2,3], Peng R. Chen[1] and Yi Rao[1,2,3,#]

[1]Laboratory of Neurochemical Biology, Peking-Tsinghua Center for Life Sciences, Peking-Tsinghua-NIBS (PTN) Graduate Program, School of Life Sciences; Department of Chemical Biology, College of Chemistry and Chemical Engineering; School of Pharmaceutical Sciences, PKU-IDG/McGovern Institute for Brain Research, Peking University, Beijing, China.

[2]Chinese Institute of Brain Research, Beijing (CIBR), and Chinese Institutes for Medical Research, Beijing (CIMR), Capital Medical University, Beijing, China.

[3]Changping Laboratory, Yard 28, Science Park Road, Changping District, Beijing, China, Research Unit of Medical Neurobiology, Chinese Academy of Medical Sciences, Beijing 102206, and Institute of Physiology, Shenzhen Bay Laboratory, Shenzhen, Guangdong, China.

*These are co-first authors.

[#]Corresponding Author (email: yrao@pku.edu.cn)

Understanding of sleep mechanisms traditionally rely on electrophysiology and genetics but here we have initiated biochemical and chemical biological studies. Sleep was increased in mouse mutants with an alanine replacing threonine at residue 469 (T469A) of the salt inducible kinase 3 (SIK3). We searched for T469 phosphatases by classic purification with HEK293 cells and by a new photo-crosslinking method with mouse brains. Both led to PPP3CA, a catalytic subunit of calcium/calmodulin activated phosphatase (calcineurin). It dephosphorylated T469 and serine (S) 551 but not T221 in SIK3 in vitro. PPP3CA knockdown increased phosphorylation of T469 and S551 but not T221 in mouse brains. Knockdown of its regulatory subunit PPP3R1 significantly reduced daily sleep by more than 5 hours, exceeding other known mouse mutants. Our results have uncovered in vitro and in vivo evidence for site-specific SIK3 dephosphorylation by calcineurin, demonstrated a physiological role for calcineurin in sleep, and suggested sleep control by calcium dependent dephosphorylation.

Sleep is an important physiological process in animals[1]. It is regulated by the circadian and the homeostatic processes[2,3]. The genetic approach has been taken in flies, mice, dogs and humans and proven powerful in uncovering many genes involved in sleep regulation[4-11]. Prominent examples include the discoveries of roles of orexin and its receptor in maintaining wakefulness[12,13], and the finding of salt inducible kinase 3 (SIK3) through a forward genetic screen[14]. No attempt has been made to use biochemistry as a means of discovering molecules important for sleep because sleep could only be assayed in animals which are accessible to genetics, but not on molecules only biochemically accessible.

While we have taken the genetic approach in both Drosophila[15-18] and the mouse[10,17,19], we assessed its advantages and limits and decided to use both a biochemical approach with the classic purification method and a chemical biological approach with a newly developed chemical biological method to investigate molecular mechanisms of sleep by examining site-specific phosphorylation of a protein kinase previously found to be important for sleep regulation[14,19-21].

Protein phosphorylation differs between day and night and among different sleep-wake relevant states[22-25]. Multiple protein kinases in mammalian animals have been implicated in sleep regulation, including protein kinase A (PKA)[26-30], the extracellular signal-regulated kinase (ERK)[31-33], adenosine monophosphate (AMP)-activated protein kinase (AMPK)[34-36], calcium (Ca^{2+})/calmodulin (CaM) kinase II (CaMKII) α and β[37–39], c-Jun N-terminal kinase (JNK)[40], SIK 3, 1 and 2[14,19-21], and the liver kinase

B (LKB1)[17,41-43]. A role for Ca^{2+}-dependent pathway in regulating sleep has been proposed[38] and was thought to be mediated at least in part by CaMKII α and β[38,39]. The reduction of sleep per 24 hours (hrs) was more than 120 minutes (mins) in CaMK2β knockout mice[38], which was more than other known genetic mutants in mice[10,12-14,17,19,21,27,30,39,44-53].

While kinases are well known to play roles in mammalian sleep, little is known about protein phosphatases (PPases) in mammalian sleep. A protein discovered in the 1970s[54-56] was named calcineurin (CaN, PP2 or PPP3)[57] before its function as a phosphatase was characterized in the 1980s[58,59]. By the 1990s, most of biochemical properties of CaN were known, such as that it is the only Ca^{2+}- and calmodulin (CaM)-activated phosphatase, that the enzyme is a dimer made of a catalytic subunit calcineurin A (with three alternatives, PPP3CA, PPP3CB or PPP3CC) and a regulatory subunit calcineurin B (with two alternatives PPP3R1 or PPP3R2)[60-62]. PPP3CA, PPP3CB and PPP3R1 are ubiquitously expressed, whereas PPP3CC is abundant in the testis and PPP3R2 is specifically expressed in the testis. Loss of either PPP3CC or PPP3R2 leads to male infertility[63-68]. CaN functions in many systems, with its role in immunoregulation particularly striking[69-72]. Recently, the number of potential targets for all forms of calcineurin expanded from approximately 70 to 486 proteins[72]. In the brain, PPP3CA is the most abundant of the three catalytic subunits and PPP3R1 is the most abundant of the two regulatory subunits.

We began to search for PPases for SIK3 after defining the importance of a specific phosphorylation site in SIK3: threonine (T) 469. While loss of the serine (S) 551 equivalent sites in SIK1 and SIK2 caused the same gain of function (GOF) phenotype as that of S551 SIK3 GOF[21], deletion of SIK1 or SIK2 gene did not affect sleep in mice[19]. We therefore have focused on SIK3 but not SIK1 or SIK2 in further studies. T469 and S551 of SIK3 are phosphorylated by PKA and their phosphorylation increased SIK3 interaction with the 14-3-3 protein[73]. 14-3-3 binding inhibited SIK3 and absence of either T469 or S551 increased SIK3 signaling[73]. S551 phosphorylation of SIK3 reduced sleep[14,20]. The functional significance of T469 phosphorylation in SIK3 was previously unknown. Here we have generated T to alanine (A) mutation of the amino acid residue at 469 (T469A) of SIK3. We found sleep increased in T469A mice as compared to wild type (wt) mice, indicating that the function of T469 is similar to that of S551 in sleep regulation.

We used two approaches to search for PPases of T469 and S551 of SIK3: classic biochemistry of purifying PPases for T469 and S551 of SIK3 from human embryonic kidney (HEK) HEK 293T cells, and chemical biology of photo-crosslinking of proteins (RG and PRC) interacting with SIK3 in the mouse brain. In both experiments, PPP3CA, a catalytic subunit of CaN, was found. in vitro biochemical assays demonstrated that PPP3CA dephosphorylated phospho-T469 and phospho-S551 of SIK3. This reaction also required Ca^{2+}, CaM and PPP3R1. Interestingly, PPP3CA did not dephosphorylate T221 of SIK3, a site whose phosphorylation promotes SIK3 activity[17,19] and indicates

sleep need and promotes sleep[19]. Ca^{2+} ionophore induced dephosphorylation of T469 and S551, but not T221, was inhibited in HEK cells when PPP3CA and PPP3CB or the regulatory subunit PPP3R1 was knocked down by small guided RNA (sgRNA) mediated gene knockdown. Phosphorylation of T469 and S551, but not T221, was increased in mouse brains when PPP3CA or PPP3R1 was knocked down, indicating that PPP3CA and PPP3R1 is physiologically required for dephosphorylation of T469 and S551 in vivo. Knockdown of PPP3CA reduced sleep by approximately 3 hrs (or 187.6±13.0 mins to be precise) over 24 hrs. Knockdown of PPP3R1 reduced sleep by more than 5 hrs (or 349.3±21.5 mins) per day, which exceeded sleep changes in all mouse mutants tested so far. Measured by the extent of changes in sleep, CaN is the most significant regulator of sleep identified so far. Our work is the first to rely on biochemistry and chemical biology to discover molecules important for sleep and it has shown the awesome power of biochemistry and chemical biology (in addition to that of genetics) in sleep research.

Results

Functional significance of T469 in regulating mouse sleep

To study the potential role of T469 in SIK3, we generated a line of mice carrying the T469A mutation (Fig. 1, Extended Data Figs. 1 and 2, Extended Data Tables 1 and 2). Sleep is usually measured in male mice but, because male mice with the genotype of $SIK3^{T469A/T469A}$ were embryonic lethal, we could only compare the sleep phenotypes

of two genotypes (SIK3$^{+/+}$ and SIK3$^{T469A/+}$) in males. We have also examined the sleep phenotypes of all three genotypes (SIK3$^{+/+}$ and SIK3$^{T469A/+}$ and SIK3$^{T469A/\ T469A}$) in females (Extended Data Figs. 3 and 4, Extended Data Tables 1 and 2). The phenotypes in males and females were qualitatively similar, though the phenotypes of SIK3$^{T469A/T469A}$ were stronger than those of SIK3$^{T469A/+}$, as expected.

Representative electroencephalogram (EEG) and electromyogram (EMG) graphs are shown in Fig. 1K and typical hypnograms shown in Figure S2E. Over 24 hrs, SIK3$^{T469A/+}$ males slept more than SIK3$^{+/+}$ males by 50.1±18.9 mins (Fig. 1a, Extended Data Table 2). During daytime, (or the light phase), there was no significant difference in sleep time between SIK3$^{T469A/+}$ and SIK3$^{+/+}$ males (Fig. 1a, Extended Data Table 2, 7.7±9.7 mins). During nighttime (or the dark phase), SIK3$^{T469A/+}$ males slept more than SIK3$^{+/+}$ males by 42.4±15.1 mins (Fig. 1a, Extended Data Table S). The amount of total non-rapid eye movement (NREM) sleep during 24 hrs was increased in SIK3$^{T469A/+}$ males by 55.8±17.5 mins over SIK3$^{+/+}$ males (Fig. 1 b and c). The amount of nighttime NREM sleep was increased in SIK3$^{T469A/+}$ males by 40.6±13.6 mins over SIK3$^{+/+}$ males (Fig. 1 b and c). Neither NREM episode number nor episode duration reached statistical significance (Fig. 1 d and e). Rapid eye movement (REM) sleep was not significantly different between SIK3$^{T469A/+}$ and SIK3$^{+/+}$ males (Extended Data Fig. 1 e-g, Extended Data Table 2). Power spectrum of EEG showed only increase in the 0.5 to 3 Hertz (Hz) range (Fig. 1f). Sleep need is an important regulator of sleep[2,3,74,75]. It is regulated by prior wakeful experience[2,76] and can be measured by NREM delta

power densities which is a measure of EEG activity in the 1-4 Hz range[2,74,75,77,78]. NREM delta power densities are significantly increased in SIK3$^{T469A/+}$ males (Fig. 1g). Other parameters were not significantly different between SIK3$^{T469A/+}$ and SIK3$^{+/+}$ males.

In females, SIK3$^{T469A/T469A}$ mice showed significantly more NREM sleep in the dark phase (84.6±26.5 mins more than SIK3$^{+/+}$ mice or 60.8±27.4 mins more than SIK3$^{T469A/+}$ mice) (Extended Data Fig. 3 a and b, Extended Data Tables 1 and 2), attributable to an increase of NREM episode number (Extended Data Fig. 3c) but not episode duration (Extended Data Fig. 3d). REM sleep was not significantly different in the dark phase, but decreased in the light phase (Extended Data Fig. 3 e and f, Extended Data Tables 1 and 2), attributable to the decrease of REM episode number (Extended Data Fig. 3g) but not episode duration (Extended Data Fig. 3h). Wake was decreased in the dark but not the light phase (Extended Data Fig. 3 i and j, Extended Data Tables 1 and 2). Wake episode number was increased in the dark (Extended Data Fig. 3) while wake episode duration was decreased in the dark (Extended Data Fig. 3l). Transition from NREM to REM was decreased whereas the other transitions were not different (Extended Data Fig. 3 m to p). NREM delta power densities were increased in both SIK3$^{T469A/T469A}$ and SIK3$^{T469A/+}$ females when compared to SIK3$^{+/+}$ females (Extended Data Fig. 4).

In summary, in male and female T469A mutants, both total sleep and NREM sleep in the dark phase was increased. NREM delta power densities were also increased in

both male and female T469A mutant mice. T469 phosphorylation is indeed a negative regulator of basal NREM sleep and sleep need, which are both opposite to the roles of SIK3[14,19-21].

Biochemical purification of phosphatase(s) for T469 and S551 of SIK3

With HEK 293T cells, we biochemically purified phosphatase(s) capable of dephosphorylating T469 and S551 of SIK3 (Fig. 2).

We first ensured that the antibodies we used could specifically recognize the phospho-forms of T469 and S551 of SIK3. Recombinant SIK3 fragment containing its amino acid residues (aa) 1 to 558 was generated in and purified from *Escherichia coli* (*E. coli*). The presence of both PKA and ATP catalyzed phosphorylation of T469 and S551 in vitro. When the antibodies were tested, they were each confirmed to be specific for the phosphorylated forms of T469 and S551, respectively (Extended Data Fig. 5).

We lysed HEK 293T cells and fractionated 500 mg of cell lysates (at a concentration of 10 mg/ml) sequentially on a Q HP, a Blue HP, an SP HP, a heparin HP, a hydroxyapatite (HAP) HP and a Superdex 200 column (Fig. 2 and Fig. 3a). At each step, an aliquot from each fraction was assayed for PPase activities at T469 and S551. Active fractions from one step were combined and further fractionated on the next column. Thus, fractions 10 to 13 from the Q HP column, the flow through (FL) fraction from the Blue HP column, the FL from the SP HP column, the FL from the

heparin column, and fractions 5 to 7 from the HAP HP column were each loaded onto the next column (Fig. 2).

During purification, we observed that PPase activities for T469 were highly correlated with those for S551 (Fig. 2 and Extended Data Fig. 3b).

Fractions 10 to 18 from the Superdex 200 column were run onto a polyacrylamide gel and silver-stained for proteins (Fig. 3b). Fraction 15 contained the strongest PPase activities. A thick band indicated by an arrow in the lane for fraction 15 was cut and sent for mass spectroscopic (MS) analysis. Four PPases were detected: PPP3CA, PPP3CB, PPP3CC and PPP5C (Fig. 3c).

Discovery of PPP3CA as a protein-protein interaction partner for SIK3 in the mouse brain

We used a new photo-crosslinking method invented by two of us (RG and PRC, unpublished) to search for proteins interacting with SIK3 in vivo. We intended to capture interacting proteins of SIK3 in the brain. Compared with digested neuronal cell culture or cell lysates, brain slices are better in keeping in situ protein networks. Among current approaches for studying protein-protein interactions (PPIs), photo-crosslinking strategies which covalently capture interacting proteins under light irradiation are considered to be the more desired methods in living systems due to their good temporal resolution and low cytotoxicity compared with chemical crosslinking. However, the incorporation of photo-crosslinkers into proteins of interests (POIs)

204 normally relies on genetic code expansion (GCE) strategy to engineer native tRNA
205 synthetases for photoactivable unnatural amino acid insertion[79] or metabolic turn-over
206 processes for photoactivable moiety containing amino acid analogues[80], which are
207 both difficult to achieve in tissue samples. Furthermore, traditional moieties used for
208 photo-crosslinking such as diazirine and aryl azide are normally sensitive to ultraviolet
209 (UV) irradiation[81], which possesses high-energy phototoxicity and weak tissue
210 penetration[82]. As a result, photo-crosslinking strategy for in situ PPI capture in tissue
211 level samples has not been frequently reported.

212 Based on the previous work from the Chen lab[83], here we (RG and PRC) have
213 developed a photocatalytic crosslinking strategy for capturing PPIs in mouse brain
214 slices (Fig. 4a). Considering the challenges as mentioned, we chose eosin Y as the
215 photocatalyst and 1,6-diaminohexane as the linker. Each compound shows good
216 solubility and eosin Y, in particular, is widely used in tissue staining. With maximum
217 absorption at 517 nm, eosin Y generates singlet oxygen ($^1O_2$) under green light
218 irradiation[84], which activates side chains of certain amino acid residues such as
219 tyrosine to form electrophilic intermediates which could further form covalent linkage
220 with amine warhead[85]. Our method does not require transfection or genetic
221 modification to incorporate the photocatalyst or the crosslinker into target samples for
222 PPI capture.

We have generated SIK3-3xHA mice in which the SIK3 protein was tagged with a hemagglutinin (HA) epitope at its carboxyl (C) terminus[86]. This allowed us to examine proteins associated with SIK3-HA after photo-crosslinking (Fig. 4b).

We applied the photocatalytic crosslinking strategy in freshly prepared mouse brain slice samples of the SIK3-HA mice. Eosin and 1,6-diaminohexane were incorporated into samples following the protocol described, followed by green LED (GL) irradiation. The SIK3 interactome was verified by Western analysis, of which clear crosslinking bands were presented in the +GL group, indicating efficient activation of our probes (Fig. 4b).

For both crosslinking and non-crosslinking groups, SIK3 protein was enriched by anti-HA beads and the crosslinking interactome could be pulled down at the same time. For further analysis of the proteins in crosslinking complexes, we excised bands with molecular weight larger than SIK3 for MS sample preparation. Quantitative studies were performed by applying dimethyl labeling method towards both groups after trypsin digestion. Although there were individual variations, 81 proteins overlapped in three independent experiment replications with high level of enrichment in the +GL groups (ratio +GL/-GL>4, log2(+GL/-GL)>2), just as shown in the Venn diagram (Fig. 4c). To better justify the protein candidates, we applied a volcano plot analysis (Fig. 4d), in which only the proteins with fold-change more than 4 and p-value less than 0.05 were considered as significant interacting candidates of SIK3. There was only one catalytic PPase: PPP3CA (Fig. 4d).

To confirm interaction of SIK3 and PPP3CA in the brain, we used antibodies for SIK3 in an immunoprecipitation experiment and found both SIK3 and PPP3CA in the precipitates (Fig. 4e). Similarly, both PPP3CA and SIK3 were found in the precipitates when anti-PPP3CA antibodies were used to immunoprecipitate brain lysates (Fig. 4f). This interaction could be recapitulated in HEK 293T cells when FLAG tagged SIK3 and HA tagged PPP3CA were introduced into HEK cells and immunoprecipitation experiments carried out with either the anti-FLAG (Fig. 4g) or the anti-HA (Fig. 4h) antibodies.

in vitro Dephosphorylation of T469 and S551, but not T221 by PPP3CA

While the biochemical approach has uncovered 4 PPases with potential activities on SIK3, and the chemical biological approach has uncovered PPP3CA as an interacting protein for SIK3, it was unclear which PPase(s) could dephosphorylate SIK3 at T469 or S551. Given the widely known assumption that PPases are notoriously "non-specific", it was also unclear whether any of the PPases identified by us was specific.

We immunoprecipitated FLAG tagged SIK3 expressed in HEK 293T cells as the substrate for testing PPases because it was phosphorylated at T221, T469 and S551 (Fig. 5a). Each of the PPases (PPP3CA, PPP3CB, PPP3CC, PPP5C and PPP3R1) was also expressed in and immunoprecipitated from HEK cells. T469 and S551 of SIK3 could be dephosphorylated by PPP3CA, PPP3CB and PPP3CC, in the presence of PPP3R1. By contrast, PPP3CA, PPP3CB and PPP3CC could not dephosphorylate

T221 of SIK3. Under the same conditions, PPP5C could not dephosphorylate T469, S551 or T221 of SIK3 (Fig. 5a).

Because PPP3CA and PPP3R1 are abundant in the brain while PPP3CC and PPP3R2 are thought to be enriched or specific in the testis[63-68], we focused on PPP3CA and PPP3R1. In the presence of PPP3R1, PPP3CA immunoprecipitated from HEK cells could dephosphorylate MEK1 at S217, but not T308 of AKT1, S241 of PDK1, T215 of MARK1, S9 of GSK3β, T183 of JNK1, T185 of ERK2 (Fig. 5 b-e).

Experiments in Fig. 5 a to e used enzymes immunoprecipitated from HEK cells and it could not be ruled out that they contained other proteins associated with the intended PPase. We expressed CaM, PPP3CA and PPP3R1 in *E. coli* so that the absence of protein serine/threonine PPases in *E. coli* made the contamination impossible. We found that CaM, PPP3CA, PPP3R1 and Ca^{2+} were all required for dephosphorylation of T469 and S551 of SIK3 (Fig. 5f). This further showed that CaN is a Ca^{2+}/CaM-activated PPase requiring both its catalytic PPP3CA subunit and regulatory PPP3R1 subunit.

Thus, our in vitro results have demonstrated that PPP3CA is highly specific, because not only it does not dephosphorylate tested kinases other than SIK3 and MEK1, but it also targets T469 and S551 but not T221 in SIK3.

in vivo Requirement of PPP3CA and PPP3R1 for dephosphorylation of T469 and S551, but not T221 in HEK cells

We investigated whether PPP3CA could dephosphorylate T469 and S551 of SIK3 in HEK293T cells.

Ionomycin is a classic Ca^{2+} ionophore, allowing Ca^{2+} flow into cells. When applied to media culturing HEK cells, ionomycin could dephosphorylate T469 and S551 of SIK3 in a dose- (Fig. 6a) and time- (Fig. 6b) sensitive manner. It was also specific without evidence for changes in SIK3-T221 phosphorylation (Fig. 6 a-b).

Overexpression of PPP3CA/PPP3R1 enhanced the ionomycin induced dephosphorylation of T469 and S551 in a dosage-dependent manner (Fig. 6c). However, overexpression of an inactive form of PPP3CA, PPP3CA-H151A (with histidine, or H, mutated to A), did not dephosphorylate T469 and S551 (Fig. 6d).

To investigate calcineurin dependence of ionomycin induced dephosphorylation, we used sgRNAs to generate single or double knockout HEK293T cell lines for PPP3CA, PPP3CB and PPP3R1. The phenotype of single knockout for PPP3CA or PPP3CB in HEK cells was variable. However, phenotypes of PPP3CA and PPP3CB double knockout, or PPP3R1 single knockout, in HEK cells was robust. The ionomycin induced dephosphorylation of T469 and S551 of SIK3 was significantly inhibited by PPP3R1 knockout or PPP3CA and PPP3CB double knockout in HEK cells (Fig. 6e). Again, the effect was specific as phosphorylation of T221 of SIK3 was not significantly affected in any of these knockout HEK cells.

in vivo Requirement of PPP3CA and PPP3R1 for dephosphorylation of T469 and S551, but not T221, in the mouse brain

To investigate their in vivo roles in the mouse, we used the CRISPR-Cas9 strategy to target PPP3CA or PPP3R1 in the brains of adult mice, with three sgRNAs for each gene (Extended Data Fig. 6). There were two types of controls: WT^{Ctrl} were wt mice injected with the same viruses as those for targeting PPP3CA or PPP3R1; $eGFP^{Ctrl}$ were mice with Cas9 expressed from the Rosa26 locus ($Rosa^{Cas9/+}$) injected with sgRNAs targeting the enhanced green fluorescent protein (eGFP). PPP3CA knockdown ($PPP3CA^{KD}$) mice were generated by injecting $Rosa^{Cas9/+}$ mice with AAV2/PHP.eB-CMV-mScarlet-PPP3CA-sgRNA-WPRE. $PPP3R1^{KD}$ mice were generated by injecting $Rosa^{Cas9/+}$ mice with AAV2/PHP.eB-CMV-mScarlet-PPP3R1-sgRNA-WPRE.

Knockdown efficiency was examined by Western analysis, which showed that sgRNAs targeting PPP3CA or PPP3R1 readily decreased their protein levels. Furthermore, when PPP3CA was targeted by sgRNA, levels of PPP3CA and PPP3R1 proteins were reduced (Fig. 7a), showing interdependence of the catalytic and the regulatory subunits. However, PPP3CB protein level was not reduced in $PPP3CA^{KD}$ mice (Fig. 7a), indicating the specificity of sgRNAs for PPP3CA over PPP3CB. In $PPP3R1^{KD}$ mice, levels of PPP3R1, PPP3CA and PPP3CB were reduced (Fig. 7b), again confirming the interdependence of catalytic and regulatory subunits.

Levels of phosphorylation of different S/T sites of multiple proteins were examined by Western analysis. Phosphorylation levels of T469 and S551 in SIK3 were both increased after PPP3CA or PPP3R1 was knocked down in mouse brains while phosphorylation level of T221 in SIK3 was not significantly changed (Fig. 7 a and b).

We also examined phosphorylation of other protein kinases in the mouse brain. After PPP3CA or PPP3R1 was knocked down, no significant change was consistently observed for the phosphorylation level of specific S/T sites on other proteins such as T202 of ERK1/2, S217 of MEK1, T183 of JNK, S473 of AKT1, T172 of AMPKα, T286 of CaMK2α/β, S241 of PDK1, or S9 of GSK3β (Fig. 7 a and b).

These results provide in vivo evidence that CaN does not dephosphorylate specific S or T in at least 8 other kinases, and that it is specifically required for the dephosphorylation of T469 and S551, but not T221, of SIK3. Our findings that PPP3CA could dephosphorylate S217 of MEK1 precipitated from HEK cells, but that MEK1-S217 phosphorylation was not affected in PPP3CA^{KD} brains, suggest that other PPases are more important than PPP3CA in regulating the phosphorylation of S217 of MEK1 in the brain.

in vivo Physiologically requirement of PPP3CA for sleep

To investigate physiological roles of the endogenous PPP3CA in mice, we analyzed the sleep phenotypes of $PPP3CA^{KD}$ mice and compared them with those of control (WT^{Ctrl} and $eGFP^{Ctrl}$) mice.

Representative EEG and EMG graphs are shown in Figure 8K and representative hypnogram shown in Figure S8E. There is no significant difference among the three genotypes in terms of the general patterns of EEG or EMG, indicating that $PPP3CA^{KD}$ did not generally or non-specifically disrupt EEG or EMG recordings.

Total sleep over 24 hrs was significantly reduced in $PPP3CA^{KD}$ mice, with reduction at every time point in both daytime (the light phase) and nighttime (the dark phase) (Fig. 8a and Extended Data Fig. 7 a-d, Extended Data Tables 3 and 4). Differences in total sleep over 24 hrs were: 187.6±13.0 mins less in $PPP3CA^{KD}$ than $eGFP^{Ctrl}$ mice, 192.6±14.7 mins less in $PPP3CA^{KD}$ than WT^{Ctrl}, 5.0±15.1 mins more in $eGFP^{Ctrl}$ than WT^{Ctrl}. In other words, $PPP3CA^{KD}$ mice slept approximately 3 hrs less than either $eGFP^{Ctrl}$ or WT^{Ctrl} control mice. Differences of sleep duration in the 12 hrs of light phase were: 79.5±7.7 mins less in $PPP3CA^{KD}$ than $eGFP^{Ctrl}$ mice, 84.2±8.7 mins less in $PPP3CA^{KD}$ than WT^{Ctrl}, 4.8±8.9 mins more in $eGFP^{Ctrl}$ than WT^{Ctrl}. Differences of sleep duration in the 12 hrs of dark phase were: 108.1±10.3 mins less in $PPP3CA^{KD}$ than $eGFP^{Ctrl}$ mice, 108.4±11.6 mins less in $PPP3CA^{KD}$ than WT^{Ctrl}, 0.2±11.9 mins more in $eGFP^{Ctrl}$ than WT^{Ctrl}.

NREM sleep was similar to total sleep in that it was significantly reduced throughout the entire 24 hrs (Fig. 8 b and c, Extended Data Tables 3 and 4). Differences

in NREM sleep over 24 hrs were: 201.0±12.4 mins less in PPP3CA^{KD} than eGFP^{Ctrl} mice, 207.0±14.0 mins less in PPP3CA^{KD} than WT^{Ctrl}, 5.9±14.4 mins less in eGFP^{Ctrl} than WT^{Ctrl}. In other words, NREM was reduced by approximately 204 mins in PPP3CA^{KD} mice as compared to either control. Differences in NREM sleep in the light phase were: 100.8±7.6 mins less in PPP3CA^{KD} than eGFP^{Ctrl} mice, 104.9±8.5 mins less in PPP3CA^{KD} than WT^{Ctrl}, 4.1±8.8 mins less in eGFP^{Ctrl} than WT^{Ctrl}. During daytime, NREM episode number was not changed (Fig. 8d), but NREM episode duration was reduced (Fig. 8e). Differences in NREM sleep in the dark phase were: 100.2±9.2 mins less in PPP3CA^{KD} than eGFP^{Ctrl} mice, 102.0±10.4 mins less in PPP3CA^{KD} than WT^{Ctrl}, 1.8±10.7 mins less in eGFP^{Ctrl} than WT^{Ctrl}. During nighttime, the number (Fig. 8d) but not the duration (Fig. 8e) of NREM episodes was reduced.

Changes in REM sleep was much more moderate and were in opposite directions in the light vs the dark phase. Differences in REM sleep over 24 hrs were: 13.3±2.6 mins more in PPP3CA^{KD} than eGFP^{Ctrl} mice, 14.4±2.9 mins more in PPP3CA^{KD} than WT^{Ctrl}, 1.0±3.0 mins more in eGFP^{Ctrl} than WT^{Ctrl}. In other words, REM was increased by approximately 13 mins in PPP3CA^{KD} mice as compared to either control. Differences in REM sleep in the light phase were: 21.3±2.3 mins more in PPP3CA^{KD} than eGFP^{Ctrl} mice, 20.7±2.6 mins more in PPP3CA^{KD} than WT^{Ctrl}, 0.5±2.7 mins less in eGFP^{Ctrl} than WT^{Ctrl} (Extended Data Fig. 7 e and f). In other words, REM sleep was moderately (but statistically significantly) increased during daytime by approximately 20 mins, due to increased REM episode number (Extended Data Fig. 7g) but not REM

episode duration (Extended Data Fig. 7h) in $PPP3CA^{KD}$ mice. Differences in REM sleep in the dark phase were: 7.9±1.6 mins less in $PPP3CA^{KD}$ than $eGFP^{Ctrl}$ mice, 6.3±1.8 mins less in $PPP3CA^{KD}$ than WT^{Ctrl}, 1.6±1.8 mins more in $eGFP^{Ctrl}$ than WT^{Ctrl} (Extended Data Fig. 7 e and f). In other words, REM sleep was weakly decreased in nighttime by approximately 6 mins (Extended Data Fig. 7 e and f), due to decreased number (Extended Data Fig. 7g) and duration (Extended Data Fig. 7h) of REM episodes.

EEG power spectrum analysis showed only NREM delta power densities reduced in $PPP3CA^{KD}$ mice at ZT15 and ZT23 but not other time points (Fig. 8 e and f). Probabilities of transition between different sleep and wake states were increased between REM and NREM, but decreased between wake and NREM (Figure 8 i and h, Extended Data Fig. 7 k and l).

After 6 hrs of SD, NREM (Fig. 8j) or total sleep/wakefulness (Extended Data Figure 8a) recovered gradually in WT^{Ctrl} and $eGFP^{Ctrl}$ mice, whereas their recoveries after SD was significantly reduced in $PPP3CA^{KD}$ mice. Recovery of REM after SD was not significantly different among WT^{Ctrl}, $eGFP^{Ctrl}$ and $PPP3CA^{KD}$ mice (Extended Data Fig. 8b).

Thus, PPP3CA is physiologically required for basal sleep mainly by promoting NREM episode duration during daytime and NREM episode number during nighttime. PPP3CA regulation of REM was moderate and different between daytime and nighttime. PPP3CA is also physiologically required for recovery of NREM after SD.

in vivo Physiologically requirement of PPP3R1 for sleep

PPP3CA is a catalytic subunit of the CaN phosphatase. Its involvement in sleep naturally begs the question whether a regulatory subunit is also involved. Because PPP3R2 was specifically expressed in the testis, not in the brain, we investigated PPP3R1 for potential roles in regulating sleep.

Western analysis of whole brains showed that PPP3R1^{KD} mice expressed PPP3R1 protein at a significant decreased level (Fig. 7b). Representative EEG and EMG graphs are shown in Fig. 9k and representative hypnograms in Extended Data Fig. 10e.

Sleep duration at every ZT in both light and dark phases except 5 ZT hrs around light to dark transition was significantly and dramatically decreased in PPP3R1^{KD} mice (Fig. 9a and Extended Data Fig. 9 a-d, Extended Data Tables 5 and 6). PPP3R1^{KD} mice spent significantly reduced amount of time for sleep over 24 hrs: 236.4±24.5 mins for PPP3R1^{KD} mice (Extended Data Table 5). This is 381.4±22.8 mins less than eGFP^{Ctrl} mice or 349.3±21.5 mins less than WT^{Ctrl} mice (Extended Data Table 6). In other words, sleep over 24 hrs is decreased by more than 5 hrs in PPP3R1^{KD} mice.

Over 24 hrs, NREM was reduced from 543.6±6.5 mins in eGFP^{Ctrl} or 512.0± 0.6 mins in WT^{Ctrl} to 183.6±18.3 mins in PPP3R1^{KD} mice (Fig. 9c, Extended Data Table 5). This is 360.1±18.5 mins less in PPP3R1^{KD} than eGFP^{Ctrl} mice or 328.4±17.5 mins less than WT^{Ctrl} mice (Extended Data Table 6). The decrease in total NREM over 24

hrs was attributable to shorter NREMS episode duration (Fig. 9c) but not to episode number (Fig. 9d).

In the light phase, NREM sleep (Figs 9 b-e; Extended Data Tables 5 and 6) was significantly decreased in $PPP3R1^{KD}$ mice whereas REM was not significantly different between $PPP3R1^{KD}$ and $eGFP^{Ctrl}$ mice or $PPP3R1^{KD}$ and WT^{Ctrl} mice (Extended Data Fig. 9 e-h; Extended Data Tables 5 and 6). NREM of $PPP3R1^{KD}$ mice in the light phase is 212.9±14.5 mins less than $eGFP^{Ctrl}$ mice or 213.4±13.7 mins less than WT^{Ctrl} mice (Extended Data Table 6). In the dark phase, sleep of any kind (including both REM and NREM) was dramatically reduced in $PPP3R1^{KD}$ mice: 20.4±8.5 mins total sleep, 18.47±7.7 mins of NREM sleep, 1.9±0.9 mins of REM sleep (Extended Data Table 5), corresponding to a reduction of 159.0±14.1 mins less than $eGFP^{Ctrl}$ mice or 123.8±13.3 mins less than WT^{Ctrl} mice, 147.2±13.2 mins less than $eGFP^{Ctrl}$ mice or 115.0±12.5 mins less than WT^{Ctrl} mice, 11.7±2.0 mins less than $eGFP^{Ctrl}$ mice or 9.0±1.8 mins less than WT^{Ctrl} mice (Extended Data Table 6). These results indicate that PPP3R1 is physiologically required for sleep.

Probabilities of transition between different sleep and wake states (Fig. 9i) were summarized from data in Figure 9H and Figure S9K and S9L. Probabilities of transition from Wake to NREMS, and from NREMS to NREMS, were reduced whereas probabilities of transition from NREMS to wake, wake to wake were increased.

PPP3R1^{KD} mice showed neither NREMS nor REMS sleep recovery after 6 hrs of SD, with statistically significant decreases at every time point tested from the 8th to the 24th hr (Fig. 9j and Extended Data Fig. 10 a-b).

NREM delta power densities were decreased in PPP3R1^{KD} mice (Fig. 9 f-g and Extended Data Fig. 9 i-j), suggesting that PPP3R1 is required for sleep need. After SD, NREMS delta power recovery was also less in PPP3R1^{KD} mice than control mice (Extended Data Fig. 10 c-d).

Discussion

We conclude that CaN plays a major role in controlling sleep, especially of the NREM type, and suggest a signaling pathway involving not only protein kinases but also protein phosphatases in sleep regulation. Our results have also demonstrated the specificity of CaN in phosphorylating specific S and T sites in SIK3, revealing a specificity previously unsuspected for PPases.

Of the three catalytic subunits of CaN, all are active in vitro in biochemically dephosphorylating T469 and S551, but not T221, of SIK3. in vivo, we have proven a biochemical role of dephosphorylating T469 and S551 for PPP3CA and PPP3CB in HEK cells and for PPP3CA in the mouse brain. We have found a physiological role for PPP3CA in regulating sleep in the mouse. PPP3CB is also involved in HEK cells in mediating dephosphorylation induced by Ca^{2+}, but it remains to be tested whether PPP3CB is required in the brain, where it is also expressed, though at a level lower

than that of PPP3CA. The finding that the effect of PPP3R1 knockdown in the mouse was stronger than PPP3CA knockdown, especially on NREM sleep, supports the possibility that PPP3R1 also functions with a catalytic subunit other than PPP3CA. PPP3CB provides the obvious candidate. The expression of PPP3CC is thought to be testis-enriched or -specific, and its role in sleep has not been tested. Of the two regulatory subunits, we have shown biochemically that PPP3R1 is required for SIK3 dephosphorylation in HEK cells and in the mouse brain, and physiologically that PPP3R1 is required for sleep regulation. We have not targeted PPP3R2 in the mouse because it is testis-specific. Because of the interdependence of catalytic and regulatory subunits (Fig. 7 a-b), the sleep phenotypes observed by us in the manuscript should be attributed to CaN, not distinguishing among different subunits.

Is SIK3 the only downstream target mediating the physiological role of CaN in sleep regulation? It is not clear at the moment. The possibility that CaN may involve substrates in addition to SIK3 is supported by the following: the sleep phenotypes of $PPP3CA^{KD}$ and $PPP3R1^{KD}$ were stronger than that of $SIK3^{T469A/T469A}$ mutant mice, which could be explained by either more sites in SIK3 for PPP3CA dephosphorylation, or by more substrates in addition to SIK3 for PPP3CA dephosphorylation. SIK 1, 2, 3 are all members of the AMPK related kinases (ARKs), we are actively examining whether and which one of the 16 to 20 ARKs [87-89] is involved in sleep. Direct effects of CaN on targets other than ARKs are also being explored.

Advantage of combining classic biochemistry with new chemical biology

We have used both a classic biochemical purification method and a new chemical biological photo-crosslinking method. This combination is very helpful. With the biochemical method (Figs. 2 and 3), 4 PPases were purified. It was unclear which one among those 4 was the right phosphatase and it was also possible that there were other PPases. With the photo-crosslinking method, PPases were not the most prominent proteins found to interact with SIK3-HA in the brain. However, when we looked at both results, it immediately drew our attention to one PPase: the one shared by both methods.

The combination thus expediated the process of focusing on CaN as the PPase for T469 and S551 of SIK3.

A new photo-crosslinking strategy

We (RG and PRC) have developed a new photo-catalytic crosslinking strategy for capturing in situ protein-protein interactions in native tissue slice samples (Fig. 4). Our method utilizes eosin as photocatalyst which generates singlet oxygen upon visible light irradiation. The singlet oxygen activates a diamine probe to capture direct protein-protein interactions. Proteins of interest (POIs) and their interacting partners could then be pulled down and analyzed by mass spectrometry.

This method has several unique advantages: 1) it does not require transfection or other genetic methods to introduce crosslinking probes. Ready-to-use in native

511 samples and captures in situ protein-protein interactions; 2) the photocatalyst eosin
512 generates singlet oxygen with high efficiency under irradiation. The molecule itself
513 also performs high compatibility in tissue samples as a tissue staining dye; 3) the peak
514 excitation wavelength of eosin is around 520 nm. Visible light-meditated crosslinking
515 method shows benefit against traditional UV methods with better tissue penetration
516 and less cytotoxicity.
517
518 **Specificity of CaN dephosphorylation of sites in SIK3**
519 With the background of the widely held perception of PPases being not very specific,
520 the selectivity of a PPase for different sites in the same substrate protein was striking.
521 We have three pieces of in vitro evidence supporting the specificity of CaN
522 (PPP3CA and PPP3R1): 1) PPP3CA expressed in and purified by
523 immunoprecipitation from HEK cells dephosphorylated T469 and S551, but not T221,
524 of SIK3 (Fig. 5); 2) With each protein component expressed in and purified from *E.*
525 *coli*, we have demonstrated that dephosphorylation of T469 and S551 in SIK3 requires
526 Ca^{2+}, CaM, PPP3CA and PPP3R1 (Fig. 5f); 3) The same purified components
527 combined together did not dephosphorylate T221 of SIK3. CaN also did not
528 dephosphorylate T308 of AKT1, S241 of PDK1, T215 of MARK1, S9 of GSK3β,
529 T183 of JNK1, or T185 of ERK2, though it dephosphorylated S217 of MEK1 (Fig. 5
530 b-e).

We have three pieces of in vivo evidence supporting the specificity of CaN: 1) Overexpression of CaN in HEK cells enhanced Ca^{2+} ionophore induced dephosphorylation of T469 and S551 in SIK3, but did not affect phosphorylation of T221 in SIK3 (Fig. 6 c-d); 2) Knockdown of the catalytic or the regulatory subunits of CaN in HEK cells inhibited the T469 and S551 dephosphorylation induced by Ca^{2+} ionophore (Fig. 6e). Two subunits of CaN (PPP3CA and PPP3CB) had to be targeted by sgRNAs at the same time to suppress the dephosphorylation effective and robustly, suggesting that, in HEK cells, both catalytic subunits function in mediating the ionophore response. 3) This is not the case in the mouse brain where PPP3CA is highly expressed. Knockdown of PPP3CA alone was sufficient to inhibit the dephosphorylation of T469 and S551 of SIK3 (Fig. 7a). PPP3CA knockdown did not affect the phosphorylation level of T221 of SIK3, proving the site-specificity of CaN for SIK3. PPP3CA or PPP3R1 knockdown in the mouse brain also did not affect the phosphorylation of specific sites in kinases such as ERK1/2, MEK1, JNK, AKT, CaMK2α/β, PDK1, or GSK3β (Fig. 7 a-b).

The specificity of CaN for T469 and S551 of SIK3 raises the question whether there is a site specific PPase for T221 of SIK3. More broadly, are there kinase-phosphatase pairs in all important signaling pathways?

CaN regulation of sleep

PPP3CA knockdown reveals that it is required physiologically for regulating sleep both during daytime and nighttime, especially NREM (Fig. 8 a-e). Its role in REM sleep is moderate and different between daytime and nighttime (Extended Data Fig. 7 e-h). Different from LKB1[17] or SIK3[19] knockout mice, sleep need measured by NREM delta power densities was not affected by PPP3CA knockdown (Fig. 8 f and g). PPP3CA is required for recovery of NREM sleep (Fig. 8j), but not REM sleep (Extended Data Fig. 8b), after deprivation, indicating that PPP3CA is important for homeostatic regulation of sleep.

PPP3R1 knockdown showed a stronger phenotype than PPP3CA, which is expected because a regulatory subunit can interact with all catalytic subunits in the brain, while, although the catalytic subunit could also interact with all regulatory subunit, there is only one regulatory subunit in the mouse brain, with the other one (PPP3R2) limited to the testis.

PPP3R1 is required physiologically for both NREM and REM sleep. It is required for nighttime sleep, and its reduction led to near elimination of NREM and REM sleep at nighttime (Fig. 9 a-c; Extended Data Fig. 9 e-f). During daytime, it is required more for NREM sleep (Fig. 9 b-c; Extended Data Fig. 9 e-f). It is required for sleep need indicated by NREM delta power densities (Fig. 9g), and for recovery of both NREM (Fig. 9j) and REM (Extended Data Fig. 10b) after SD.

Calcium regulation of sleep

572 Ca^{2+} imaging in different brain regions have shown that intracellular and extracellular
573 concentrations of Ca^{2+} are different among different sleep/wake states[90-93].
574 Pharmacological and genetic manipulations of channels affecting Ca^{2+} concentrations
575 could change sleep patterns in mice[38,94-97].

576 Our findings of the roles of CaN provides one possible downstream component of
577 Ca^{2+}, but it remains to be further studies how Ca^{2+}, kinases, phosphatases, ion channels
578 and transcriptional factors interact in sleep regulation.

579

580 **Protein kinases and sleep**

581 The first kinase implicated in sleep regulation was PKA. An antidepressant capable of
582 inhibiting phosphodiesterase and increasing cyclic adenosine monophosphate (cAMP)
583 could increase wakefulness[26] in rats. In mice, overexpression of a dominant negative
584 form of PKA increased REM sleep and NREM fragmentation while decreasing sleep
585 rebound after deprivation[30]. ERK requirement for sleep in mice was shown by
586 significant sleep reduction after pharmacological inhibitions or genetic deletions of
587 ERK1 or ERK2 genes in neurons[33]. AMPK was implicated in sleep regulation when
588 its inhibitor was found to decrease sleep and its activator found to increase sleep in
589 mice[34]. Pharmacological inhibition of CaMKII in specific brain regions was found to
590 increase sleep[37]. Genetic knockout studies show the importance of CaMK2α and
591 CaMK2β in sleep with a reduction of approximately 50 minutes (mins) or 120 mins
592 per 24 hrs in CaMK2α and CaMK2β knockout mutants, respectively[38]. SIK3 was

discovered through a forward genetic screen in mice when a gain of function mutant of SIK3 was discovered[14]. A small fragment was deleted in the SIK3^{sleepy} mutant, resulting in the absence of a PKA target site S551[20]. Mutations of the S551 equivalent sites in SIK1 and SIK2 led to the GOF phenotype[21], making it unclear which of the SIK kinases or phosphorylation sites were physiologically required for sleep regulation. Our studies of mice deleting each one of the SIK genes indicated that only SIK3, but not SIK1 or SIK2 is required for sleep in mice[19]. LKB1 is a tumor suppressor gene[41-43,98,99] whose product was found to phosphorylate T172 of the α subunit of AMPK[100-106] and the equivalent site in ARKs including SIK3[87]. Our recent functional studies in vivo have shown requirement of LKB1 for sleep in both flies and mice[17]. The simple scenario of LKB1 upstream of SIK3 in sleep regulation was rendered uncertain by our in vitro biochemical studies which has uncovered more than twenty kinases of the STE20 subfamily in addition to LKB1 upstream of ARKs[107,108]. We are still studying whether any of the STE20 kinases identified by us biochemically is involved in sleep regulation.

Our discovery of specific phenotypes for CaN in sleep will stimulate further studies of other PPases in regulating sleep. For example, while it seems that CaN is more important for NREM than REM, would there be a PPase more important for regulating REM sleep? What are the relationships between kinases and phosphatases in sleep regulation? The specificities we discovered for CaN in dephosphorylating specific sites and in regulating specific components of sleep brings both questions and

614 excitement for furthering our understanding of molecular mechanisms of mammalian
615 sleep. More broadly, specific involvement of PPases in important physiological
616 processes should be further studied.
617

Methods

Antibodies

The following primary antibodies were used: anti-HA tag (C29F4, CST), anti-FLAG M2 HRP conjugated (A8592, Sigma), anti-SIK3 (Santa Cruz, sc-515408), anti-SIK3 pT221 (Abcam, ab271963), anti–SIK3 pT469 (Abcam, ab225633), anti–SIK3 pS551 (Abcam, ab225634), anti-PPP3CA (ABclonal, A1063), anti-PPP3CB (AffinitY, DF12705), anti-PPP3CC (ABclonal, A7714), anti-PPP3R1 (ABclonal, A0954), anti-JNK (CST, 9252), anti-phospho-JNK (CST, 9251), anti-ERK1/2(CST, 4695), anti-phospho-ERK (CST, 4370), anti-AMPKα1/α2 (ABclonal, A12718), anti-AMPKα1/2–pT183/T172 (ABclonal, AP1345), anti-PDK1 (ABclonal, A8930), anti-PDK1 pS241 (ABclonal, AP1357), anti-MEK1/2 (ABclonal, A4868), anti-MEK1/MEK2 pS217/S221 (ABclonal, AP1349), anti-GSK3β (CST, 12456), anti–GSK3β pS9 (CST, 5558), anti-panAkt (CST, 4685), anti-Akt pS473 (CST, 4060), anti-CaMKII pT286 (Abcam, ab171095), anti-CaMKIIα/β (CST, 4436S), anti–β-actin (Abcam, ab8226).

Cell culture and cDNA transfection

HEK293T cells were cultured in Dulbecco's modified Eagle's medium (DMEM, Gibco) medium containing 10% fetal bovine serum (FBS, Gibco) and 1% Penicillin/Streptomycin (Gibco). cDNAs were transfected into HEK293T cells with Lipofectamine 3000 reagent (Thermo Fisher) according to the manufacturer's instructions and harvested 24 to 28 hrs after transfection.

639

640 **Drug treatment and protein preparation**

641 HEK293T cells were treated with ionomycin (MedChemExpress) at indicated
642 concentrations and time durations at 37 ℃. Cells were then harvested and lysed with
643 1 ml lysis buffer (0.3% Chaps, 10 mM KCl, 1.5 mM $MgCl_2$, 1 mM EDTA, 1 mM
644 EGTA, pH 7.4, 1x protease inhibitor cocktail (Roche), 1x phosphatase inhibitor II and
645 1x phosphatase inhibitor III (Sigma)) before centrifugation of cell lysates at 13000 rpm
646 for 10 min at 4 ℃. Protein concentrations of cell lysates were determined with the
647 bicinchoninic acid (Thermo Fisher, 23225) assay and normalized to 2 mg/ml. Samples
648 were analyzed by immunoblotting with the indicated antibodies.

649

650 **Mice**

651 WT C57 BL/6J mice (8 to 10 weeks old) were purchased from Beijing Vital River
652 Laboratories Technology Co., Ltd. or Laboratory animal resource center in Chinese
653 Institute for Brain Research. Rosa26-Cas9 knock-in ($Rosa26^{Cas9/+}$, RRID:
654 IMSR_JAX:024858) mice were obtained from Jackson laboratory [109]. SIK3-3xHA
655 mice were constructed in BIOCYTOGEN by infusing a 3xHA-T2A-iCre cassette into
656 the C terminus right before the SIK3 stop codon. All experimental procedures were
657 performed in accordance with the guidelines and were approved by the Animal Care
658 and Use Committee of Chinese Institute for Brain Research, Beijing. Mutant mice and
659 wt littermates were maintained on a C57 BL/6J background. Mice were housed under

a 12 hr:12 hr light/dark cycle and controlled temperature and humidity conditions. Food and water were delivered *ad libitum*. Mice used in all experiments were 10-14 weeks old.

Generation of mice with point mutations in SIK3

SIK3 point mutant mice were constructed with CRISPR-Cas9 mediated homologous recombination. For SIK3$^{T469A/T469A}$, the gRNA sequence was 5'-TTTGTCAATGAGGAGGCACA-3' and a single strand homologous arm was designed to introduce nucleotide mutation from ACG to GCG (T469A) as well as a restriction enzyme site *BstUI* for future genotyping, sequence of which was 5'-CCTTCTCCAGAAGCCTTGGTTCGCTATTTGTCAATGAGGAGGCACGCGGT GGGAGTGGCTGACCCACGGTAAGTACCTGGTCAGCATCCT-3'. A mixture of Cas9-expressing mRNA, single strand homologous arm and sgRNA was injected into fertilized eggs through electroporation and the eggs were then transplanted into the womb of foster mothers. F0 and F1 mice were genotyped through PCR and *BstUI* digestion to make sure the presence of recombination. Mutant lines were back-crossed to C57BL/6J for at least 5 generations to exclude possible off-targeting.

Mouse brain protein preparation

Whole brains of mice were quickly dissected, rinsed withP BS and homogenized by homogenizer (Wiggens, D-500 Pro) in ice-cold lysis buffer (150 mM NaCl, 1% Triton-

X-100, 0.5% sodium deoxycholate, 0.1% SDS, 50 mM Tris-base, freshly supplemented with a protease and phosphatase inhibitor cocktail). Brain homogenates were centrifuged at 15000 rpm for 25 min at 4 ℃. Supernatants were carefully transferred into a new microtube. Protein concentrations of brain lysates were determined with the bicinchoninic acid assay and normalized to 2 mg/ml. Before immunoblotting, samples were kept in liquid nitrogen, if necessary.

Biochemical purification

Lysates from HEK 293 cells were prepared and filtered through 0.45 μm filters. 500 mg cell lysates at a concentration of 10 mg/ml were fractionated on a QHP anionic chromatography column, eluted with a linear gradient of NaCl (0-600 mM) into 20 column volumes (CVs), with each fraction collected as one CV as samples 1 to 20, and the final wash with 1 M NaCl buffer A with 5 CVs gave rise to samples 21 to 25. Each fraction was dialyzed into buffer A, removing NaCl. 10 μl of each sample was used for analysis of activities removing phosphate from SIK3 T469 and S551. T469 and S551 of bacterially expressed recombinant SIK3 were phosphorylated by PKA in vitro before being used to test phosphatase activities of the fractions of HEK lysates. Fractions 10 to 13 contained significant activities removing phosphate from SIK3 T469 and S551.

Fractions 10 to 13 from QHP were combined and dialyzed with buffer A before being loaded onto a Blue HP column. It was eluted with a linear gradient of NaCl (0-

600 mM) into 20 column volumes (CVs), with each fraction collected as one CV as samples 1 to 20, and the final wash with 1 M NaCl buffer A with 5 CVs gave rise to samples 21 to 25. The FL fraction from the Blue HP contained significant activities removing phosphate from SIK3 T469 and S551.

The FL fraction from the Blue HP column was dialyzed with buffer A and loaded onto a SPHP column. The FL fraction from the SP-HP column contained significant activities removing phosphate from SIK3 T469 and S551.

The FL fraction from the SP-HP column was dialyzed with buffer A and loaded onto a heparin HP column. The FL fraction and Fraction 1 contained significant activities removing phosphate from SIK3 T469 and S551.

The FL fraction from the heparin HP column was dialyzed with buffer A and loaded onto a HAPHP column. The rest of the fractionation was similar to the first column except that the final wash was with 5 CVs of 500 mM K_2PO_4, giving rise to samples 21 to 25. Fractions 5 to 7 contained significant activities removing phosphate from SIK3 T469 and S551.

Active fractions from the HAPHP column were condensed into 0.5 ml, fractionated on a Superdex 200 molecular sieve column, eluted with 200 mM NaCl gradient into 20 CVs. 1 ml from each fraction was collected and labeled as samples 1 to 20. Protein contents were monitored with UV at 280 nm.

Incorporation of photocatalytic probes into mouse brain slices for visible light-induced PPI capture

SIK3-3xHA mice were sacrificed and brain slices were kept in PBS. Neurobasla medium (Gibco) supplied with B-27 for photocatalytic crosslinking was prepared in darkness by adding eosin Y and 1,6-dihexamine to a working concentration of 50 μM and 1 mM, respectively. Cell culture chambers (Millipore, PICM0RR50) were placed in 6-well plates and rinsed with PBS. Brain slices were transferred to chambers carefully with a sterile dropper and each chamber finally contained four slices to ensure thorough stretch of each slice. PBS was discarded by pipetting from the outer side of chambers and 0.5 ml of neurobasal medium containing photocatalytic crosslinkers was added into each well to ensure that each slice was totally infiltrated with the probes. Samples were incubated at 37°C with 5% CO_2 for 1 hr before photo-irradiation. For photocatalytic crosslinking, the plates were placed on green LED (520 nm, 20 mW/cm^2) equipment while an ice bag and a fan were used to reduce light irradiation-induced heat. After 15 mins of green light irradiation, the color of the medium was bleached, indicating effective activation of the eosin probe. The medium was discarded and after one round of PBS wash, the slices was collected into 1.5 ml Eppendorf tubes, which were placed into liquid N_2 to freeze the slices.

Enrichment of crosslinked proteins

742 To each tube with frozen brain slice samples was added 1 ml of ice-cold lysis buffer
743 containing 1% of protease cocktail and a steel ball. Samples were lysed through
744 ultrasonication. After centrifugation (12,000 g, 10 mins, 4 °C) to discard the residue,
745 crosslinked proteins were enriched by anti-HA magnetic beads (Pierce, 88837)
746 according to the manufacture protocol. Importantly, the beads should be washed with
747 lysis buffer (with 0, 0.25, and 0.5 M NaCl) for three times to diminish non-specific
748 binding proteins. Crosslinked proteins were eluted with 2x SDS-loading buffer and
749 heated to 95 °C for 10 min. Eluted proteins were subjected to further Western analysis
750 and LC-MS/MS.
751
752 **Protein digestion and dimethyl labeling**
753 **In-gel digestion.** Proteins enriched with HA beads were loaded on an 8% SDS-PAGE
754 gel and run at 150 V for 30 mins. After silver staining, the desired bands of protein
755 mixture were excised and cut into 1 mm^3 pieces. The gel pieces were discolored in
756 discoloring buffer until they all turned transparent. A dehydration process was carried
757 out by adding pure acetonitrile into gel pieces until they were totally dehydrated to
758 appear non-transparently white. Samples were then incubated in the reduction buffer
759 (10 mM DTT, 50 mM ammonium bicarbonate) at 56 °C for 30 mins and further
760 incubated in alkylation buffer (55 mM iodoacetamide, 50 mM ammonium bicarbonate)
761 at 37 °C for half an hr in the dark. After washed by 50 mM ammonium bicarbonate
762 buffer twice, gel pieces were dehydrated through the same protocol. 20 ng/μl trypsin

763 buffer in 50 mM ammonium bicarbonate was added and samples were incubated at
764 4 °C for one hr. The remaining buffer was discarded and 50 mM ammonium
765 bicarbonate buffer was added for another 16 hrs of digestion at 37 °C. The resulting
766 peptides were extracted with extraction buffer (50% acetonitrile, 45% water and 5%
767 formic acid), before being centrifuged to dryness under vacuum.

768 **Dimethyl labeling**. The collected peptides were reconstituted in 100 mM TEAB buffer.
769 39.688 mg/mL of $NaBH_3CN$ followed by 4% (v/v) CH2O or CD2O were added for
770 light and heavy dimethyl labeling, respectively, following the addition of 39.688
771 mg/ml $NaBH_3CN$. After incubation in a fume hood for 30 mins at room temperature,
772 enough 1% (v/v) ammonia solution and FA were added immediately to quench the
773 labeling reaction. The light and heavy samples were combined together, and then
774 desalted and dried under vacuum.

775 **LC-MS/MS analysis**. Trypsin digested peptides were analyzed on a Exploris 480
776 Hybrid Quadrupole Orbitrap Mass Spectrometer as well as Thermo Scientific Q
777 Exactive Orbitrap Mass Spectrometer in conjunction with an Easy-nLC II HPLC
778 (Thermo Fisher Scientific). The mobile phases were A: 0.1% formic acid in H_2O; B:
779 0.1% formic acid in 80% ACN–20% H_2O. MS/MS analysis was performed under the
780 cationic mode with a full-scan *m*/z range from 350 to 1,800 and a mass resolution of
781 70,000.

782 **Peptides identification.** For quantitative SIK3 interactome analysis, the quantification
783 of light/heavy ratios was calculated with a precursor mass tolerance of 20 ppm.

Alkylation of cysteine (+57.0215 Da) was set as the static modification, and oxidation of methionine (+15.9949 Da) and acetylation of N-terminal Lys (+42.0106 Da) was assigned as the variable modification. The isotopic modifications (28.0313 and 32.0557 Da for light and heavy labeling, respectively) were set as fixed modifications on the peptide N-terminus and lysine residues. Half-tryptic terminus and up to two missing cleavages were set within tolerance.

Co-immunoprecipitation: For HEK293T cells, plasmids expressing FLAG-tagged SIK3 and HA-tagged PPP3CA were transfected for 24 hrs. Cells were then collected and lysed with 1 ml lysis buffer (25 mM Tris-base pH 7.4, 150 mM NaCl, 1% NP40, 1mM EDTA, 5% glycerol,1x protease inhibitor cocktail, 1x phosphatase inhibitor II and 1x phosphatase inhibitor III) before centrifugation at 13000 rpm for 10 min at 4℃. 40 µl supernatants were transferred into new microtubes as input samples and the rest was incubated either with 20µl anti-FLAG (Millipore, M8823) or anti-HA antibody coated magnetic beads balanced by lysis buffer for 1 hr at 4 ℃. Beads were then washed with 1 ml lysis buffer three times at 4 ℃ and 40 µl PBS was added to transfer the beads into new microtubes as enriched samples. For mouse, anti-PPP3CA or anti-SIK3 antibody and corresponding IgG were pre-incubated with protein A/G beads (YEASEN) for 2 hrs at 4℃ in lysis buffer. Protein samples from mouse brain were at first pre-absorbed using IgG-protein A/G beads for 30 min at RT and 40 µl supernatants were transferred into a new microtube as input sample before anti-PPP3CA/SIK3 protein A/G beads was added and rotated overnight at 4℃. Beads were

805 then washed with 1 ml lysis buffer three times at 4℃ and 40 μl PBS was added to
806 transfer the beads into a new tube as enriched samples.
807
808 **Expression of recombinant proteins in *E. coli***
809 cDNAs for specific proteins were subcloned into the pET-28a vector, with appropriate
810 tags such as MBP, GFP or FLAG. Plasmids were transfected into *E. coli* BL21 and
811 incubated at 37 ℃ until the OD reached 0.6, when 0.5 mM of IPTG was added at 18 ℃
812 to induce protein expression for 16 hrs. Cells were collected and treated with Ni
813 column binding buffer (300 mM NaCl, 20 mM Tris-HCl, pH 7.5) containing protease
814 inhibitors and thoroughly suspended. Cells were lysed with ultrasonication before
815 centrifugation (14,000 rpm, 30 mins, 4℃). Supernatants were filtered through 0.45 μm
816 and purified by Ni beads to 90% purity. Eluted proteins were measured with Coomasie
817 blue and the rest of the proteins were stored at -80 ℃.
818
819 **in vitro Phosphatase assay**
820 Plasmids expressing FLAG-tagged SIK3 were transfected into HEK293T cells for
821 immunoprecipitation. After 24 hrs, cells were collected and lysed with 1 ml lysis buffer
822 (25 mM Tris-base pH 7.4, 150 mM NaCl, 1% NP40, 1mM EDTA, 5% glycerol,1x
823 protease inhibitor cocktail, 1x phosphatase inhibitor II and 1x phosphatase inhibitor
824 III) before centrifugation at 13000 rpm for 10 min at 4 ℃. Cell lysates were incubated
825 with 20μl anti-FLAG antibody coated magnetic beads balanced by lysis buffer for 1

826 hr at 4 ℃. Beads were washed with 1 ml lysis buffer three times at 4 ℃, before final
827 elution with 30 μl buffer A containing 2 mg/ml 3xFLAG peptide. Phosphatase
828 reactions were performed for 2 hrs at 37℃ by adding 4 μl FLAG-SIK3, 3 μg rPPP3CA,
829 3 μg rPPP3R1, 4 μg rCaM with a final concentration of 10 mM $CaCl_2$ and 20 mM
830 $MgCl_2$. Samples were analyzed by immunoblotting with the indicated antibodies.
831
832 **Viruses**
833 Viruses used in this study: AAV2/PHP.eB-CMV-mScarlet-PPP3CA-sgRNA-WPRE,
834 AAV2/PHP.eB-CMV-mScarlet-PPP3R1-sgRNA-WPRE and AAV2/PHP.eB-CMV-
835 mScarlet-eGFP-sgRNA-WPRE.
836 $PPP3CA^{KD}$ and $PPP3R1^{KD}$ mice were generated with triple-targeted CRISPR-
837 Cas9 technology [110] by virus injection. Plasmids were generated before virus package.
838 Three sgRNA sequences targeting PPP3CA or PPP3R1 were designed through VBC
839 Score (vbc-score.org) and cloned into the PM04 plasmid, and sequentially inserted
840 into pAAV-CMV-mScarlet-WPRE using Gibson assembly technology. sgRNA
841 sequences were shown as follows:
842 PPP3CA-gRNA1: GACCATAGGATGTCACACAT;
843 PPP3CA-gRNA2: GCAGTCGAAGGCATCCATAC;
844 PPP3CA-gRNA3: GAGGCTGTTCGTACTTCTAC;
845 PPP3R1-gRNA1: GCTGATGAAATTAAAAGGCT;
846 PPP3R1-gRNA2: GCGATAAGGAACAGAAGTTG;

847 PPP3R1-gRNA3: GCAGAACCCTTTAGTACAGC.

848

849 **Viral injection**

850 Mice at 8 weeks old were anaesthetized using 4-5% isoflurane (maintained at 1-2%
851 for surgery), and 100uL virus (5×10^{12} gc/ml) was injected through retro-orbital sinus
852 [111]. After two weeks to allow for expression, EEG implantation surgery was performed
853 according to the protocol published previously [51]. Mice were fixed in stereotaxic
854 (RWD Life Science, 68405) and skull was exposed. Two holes were drilled at the
855 frontal and the parietal cortex over the right cerebral hemisphere (Frontal: lateral to
856 middle 1.5mm, 1.0mm anterior to bregma; parietal: lateral to middle 1.5 mm, 1.0 mm
857 anterior to lambda). Two stainless steel screws (RWD Life Science), each soldered to
858 a short copper wire, were inserted into the holes. Two EMG wires were implanted
859 bilaterally into the neck muscle. All the copper wires were attached onto a micro-
860 connector and was fixed to the skull. After surgery, mice were single housed for five
861 days of recovery in new cages and then were placed into the special recording cage for
862 three days to habituate to the recording cables.

863

864 **EEG and EMG recording and analysis**

865 EEG and EMG data recording and analysis were performed as our previous study [17].
866 EEG and EMG data at basal sleep conditions were recorded for 2 consecutive days,
867 with a sample frequency of 200 Hz and epoch length of 4 seconds. EEG and EMG data

were initially processed using AccuSleep [112] and then were manual correction in SleepSign. EEG and EMG signals were classified into Wake (fast and low amplitude EEG, high amplitude and variable EMG), NREM (high amplitude and 1-4 Hz dominant frequency EEG, low EMG tonus) and REM (low amplitude and 6-9 Hz frequency EEG, complete silent of EMG). The state episode was defined as at least three continuous and unitary state epochs. Epoch contained movement artifacts were included in sleep duration analysis but excluded from the subsequent power spectrum analysis. For power spectrum analysis, EEG was subjected to fast Fourier transform analysis (FFT). Power spectra represents the mean ratio of each 0.25 Hz to total 0–25 Hz of EEG signals during 24 hr baseline condition. The power density of NREMs represents the ratio of delta power density (1-4 Hz) to total power (0-25 Hz) in each hour. Cumulative rebound represented cumulative changes of time in post-SD compared with relative ZT under the baseline condition. Sleep/wake transition probabilities was analyzed as described in a previous study [39]. For instance, $P_{W\ to\ NR} = N_{W\ to\ NR} / (N_{W\ to\ W} + N_{W\ to\ R} + N_{W\ to\ NR})$, $N_{W\ to\ NR}$ denotes the number of transitions that transit from wakefulness epoch to NREM sleep epoch. W: wakefulness epoch, NR：NREM epoch, R: REM epoch.

Sleep deprivation

After 2 consecutive days of EEG and EMG signals recording, mice were introduced into new cages at ZT0. Mice were gently handled or touched to keep them awake for

6 hrs of sleep deprivation, before being returned to the recording cage for another 24 hrs of recording.

Statistical analysis

All statistical analyses were performed using GraphPad Prism 9.0. One-way ANOVA was used to compare differences among more than three groups, followed by Tukey's multiple comparisons tests. Kruskal-Wallis tests were used for non-parameters tests. Two-way ANOVA was used to compare the differences between different groups with different treatments, followed by Tukey's multiple comparisons tests. Two-way ANOVA with repeated measurements (Two-way RM ANOVA) was used when the same individuals were measured on the same outcome variable more than once, followed by Tukey's multiple comparisons test. Data are presented as mean±SEM. In all cases, p values morethan 0.05 were considered not significant.

Acknowledgements

We are grateful to Dr. Juan Huang at CIBR for generating SIK3 mice, Dr. Lei zhang at CIBR instrument core for help with customizing experimental devices for EEG recording, Dr. Yuan Li for help with mouse brain slice preparation, Linghao Kong and Ruixiang Wang from the CLS and Dr. Gongzheng Zhao from the Multi-Omics Mass Spectrometry Core of Shenzhen Bay Laboratory for assistance with mouse brain MS sample processing, the National Center for Protein Sciences at Peking University for

909 access to instrumentation, and CLS, CIBR, CIMR, Changping Laboratory and the
910 Chinese Academy of Medical Sciences (2019RU003) for support.

911

912 **REFERENCES**

913 1 Keene, A. C. & Duboue, E. R. The origins and evolution of sleep. *J Exp Biol* **221**,
914 doi:10.1242/jeb.159533 (2018).

915 2 Borbely, A. A. A two process model of sleep regulation. *Hum Neurobiol* **1**, 195-
916 204 (1982).

917 3 Borbely, A. A., Daan, S., Wirz-Justice, A. & Deboer, T. The two-process model
918 of sleep regulation: a reappraisal. *J Sleep Res* **25**, 131-143 (2016).

919 4 Hendricks, J. C. *et al.* Rest in Drosophila is a sleep-like state. *Neuron* **25**, 129-
920 138 (2000).

921 5 Shaw, P. J., Cirelli, C., Greenspan, R. J. & Tononi, G. Correlates of sleep and
922 waking in Drosophila melanogaster. *Science* **287**, 1834-1837 (2000).

923 6 Sehgal, A. & Mignot, E. Genetics of sleep and sleep disorders. *Cell* **146**, 194-207
924 (2011).

925 7 Stavropoulos, N. & Young, M. W. insomniac and Cullin-3 regulate sleep and
926 wakefulness in Drosophila. *Neuron* **72**, 964-976 (2011).

927 8 Liu, Q., Liu, S., Kodama, L., Driscoll, M. R. & Wu, M. N. Two dopaminergic
928 neurons signal to the dorsal fan-shaped body to promote wakefulness in
929 Drosophila. *Curr Biol* **22**, 2114-21238 (2012).

930 9 Allada, R., Cirelli, C. & Sehgal, A. Molecular Mechanisms of Sleep Homeostasis
931 in Flies and Mammals. *Cold Spring Harb Perspect Biol* **9**, a027730 (2017).

932 10 Zhang, X., Yan, H., Luo, Y., Huang, Z. & Rao, Y. Thermoregulation-Independent
933 Regulation of Sleep by Serotonin Revealed in Mice Defective in Serotonin
934 Synthesis. *Mol Pharmacol* **93**, 657-664 (2018).

935 11 Shi, G. *et al.* Mutations in Metabotropic Glutamate Receptor 1 Contribute to
936 Natural Short Sleep Trait. *Curr Biol* **31**, 13-24 (2021).

937 12 Chemelli, R. M. *et al.* Narcolepsy in orexin knockout mice: molecular genetics
938 of sleep regulation. *Cell* **98**, 437-451 (1999).

939 13 Lin, L. *et al.* The sleep disorder canine narcolepsy is caused by a mutation in the
940 hypocretin (orexin) receptor 2 gene. *Cell* **98**, 365-376 (1999).

14 Funato, H. *et al.* Forward-genetics analysis of sleep in randomly mutagenized mice. *Nature* **539**, 378-383 (2016).

15 Qian, Y. *et al.* Sleep homeostasis regulated by 5HT2b receptor in a small subset of neurons in the dorsal fan-shaped body of drosophila. *Elife* **6**, 26519 (2017).

16 Deng, B. *et al.* Chemoconnectomics: Mapping Chemical Transmission in Drosophila. *Neuron* **101**, 876-893 (2019).

17 Liu, Z. *et al.* LKB1 is physiologically required for sleep from Drosophila melanogaster to the Mus musculus. *Genetics* **221**, iyac082 (2022).

18 Dai, X. *et al.* D-Serine made by serine racemase in Drosophila intestine plays a physiological role in sleep. *Nat Commun* **10**, 1986 (2019).

19 Li, Y. *et al.* Sleep Need, the Key Regulator of Sleep Homeostasis, Is Indicated and Controlled by Phosphorylation of Threonine 221 in Salt Inducible Kinase 3. *bioRxiv*, 2021.2011.2006.467421, doi:10.1101/2021.11.06.467421 (2021).

20 Honda, T. *et al.* A single phosphorylation site of SIK3 regulates daily sleep amounts and sleep need in mice. *Proc Natl Acad Sci U S A* **115**, 10458-10463 (2018).

21 Park, M. *et al.* Loss of the conserved PKA sites of SIK1 and SIK2 increases sleep need. *Sci Rep* **10**, 8676 (2020).

22 Luo, J., Phan, T. X., Yang, Y., Garelick, M. G. & Storm, D. R. Increases in cAMP, MAPK activity, and CREB phosphorylation during REM sleep: implications for REM sleep and memory consolidation. *J Neurosci* **33**, 6460-6468 (2013).

23 Wang, Z. *et al.* Quantitative phosphoproteomic analysis of the molecular substrates of sleep need. *Nature* **558**, 435-439 (2018).

24 Bruning, F. *et al.* Sleep-wake cycles drive daily dynamics of synaptic phosphorylation. *Science* **366**, aav3617 (2019).

25 Xu, M., Liu, X., Wang, Q., Zhu, Y. & Jia, C. Phosphoproteomic analysis reveals the effects of sleep deprivation on the hippocampus in mice. *Mol Omics* **18**, 677-685 (2022).

26 Lelkes, Z., Alfoldi, P., Erdos, A. & Benedek, G. Rolipram, an antidepressant that increases the availability of cAMP, transiently enhances wakefulness in rats. *Pharmacol Biochem Behav* **60**, 835-839 (1998).

27 Hendricks, J. C. *et al.* A non-circadian role for cAMP signaling and CREB activity in Drosophila rest homeostasis. *Nat Neurosci* **4**, 1108-1115 (2001).

28 Takemori, H., Katoh, Y., Horike, N., Doi, J. & Okamoto, M. ACTH-induced nucleocytoplasmic translocation of salt-inducible kinase. Implication in the protein kinase A-activated gene transcription in mouse adrenocortical tumor cells. *J Biol Chem* **277**, 42334-42343 (2002).

29 Joiner, W. J., Crocker, A., White, B. H. & Sehgal, A. Sleep in Drosophila is regulated by adult mushroom bodies. *Nature* **441**, 757-760 (2006).

30 Hellman, K., Hernandez, P., Park, A. & Abel, T. Genetic evidence for a role for protein kinase A in the maintenance of sleep and thalamocortical oscillations. *Sleep* **33**, 19-28 (2010).

31 Foltenyi, K., Greenspan, R. J. & Newport, J. W. Activation of EGFR and ERK by rhomboid signaling regulates the consolidation and maintenance of sleep in Drosophila. *Nat Neurosci* **10**, 1160-1167 (2007).

32 Vanderheyden, W. M., Gerstner, J. R., Tanenhaus, A., Yin, J. C. & Shaw, P. J. ERK phosphorylation regulates sleep and plasticity in Drosophila. *PLoS One* **8**, e81554 (2013).

33 Mikhail, C., Vaucher, A., Jimenez, S. & Tafti, M. ERK signaling pathway regulates sleep duration through activity-induced gene expression during wakefulness. *Sci Signal* **10**, aai9219 (2017).

34 Chikahisa, S., Fujiki, N., Kitaoka, K., Shimizu, N. & Sei, H. Central AMPK contributes to sleep homeostasis in mice. *Neuropharmacology* **57**, 369-374 (2009).

35 Nagy, S. *et al.* AMPK signaling linked to the schizophrenia-associated 1q21.1 deletion is required for neuronal and sleep maintenance. *PLoS Genet* **14**, e1007623 (2018).

36 Yurgel, M. E. *et al.* A single pair of leucokinin neurons are modulated by feeding state and regulate sleep-metabolism interactions. *PLoS Biol* **17**, e2006409 (2019).

37 Datta, S., O'Malley, M. W. & Patterson, E. H. Calcium/calmodulin kinase II in the pedunculopontine tegmental nucleus modulates the initiation and maintenance of wakefulness. *J Neurosci* **31**, 17007-17016 (2011).

38 Tatsuki, F. *et al.* Involvement of Ca(2+)-Dependent Hyperpolarization in Sleep Duration in Mammals. *Neuron* **90**, 70-85 (2016).

39 Tone, D. *et al.* Distinct phosphorylation states of mammalian CaMKIIbeta control the induction and maintenance of sleep. *PLoS Biol* **20**, e3001813 (2022).

40 Takahama, K. *et al.* Pan-neuronal knockdown of the c-Jun N-terminal Kinase (JNK) results in a reduction in sleep and longevity in Drosophila. *Biochem Biophys Res Commun* **417**, 807-811 (2012).

41 Hemminki, A. *et al.* A serine/threonine kinase gene defective in Peutz-Jeghers syndrome. *Nature* **391**, 184-187 (1998).

42 Hemminki, A. *et al.* Localization of a susceptibility locus for Peutz-Jeghers syndrome to 19p using comparative genomic hybridization and targeted linkage analysis. *Nat Genet* **15**, 87-90 (1997).

43 Jenne, D. E. *et al.* Peutz-Jeghers syndrome is caused by mutations in a novel serine threonine kinase. *Nat Genet* **18**, 38-43 (1998).

44 Parmentier, R. *et al.* Anatomical, physiological, and pharmacological characteristics of histidine decarboxylase knock-out mice: evidence for the role of brain histamine in behavioral and sleep-wake control. *J Neurosci* **22**, 7695-7711 (2002).

45 Popa, D. *et al.* Contribution of 5-HT2 receptor subtypes to sleep-wakefulness and respiratory control, and functional adaptations in knock-out mice lacking 5-HT2A receptors. *J Neurosci* **25**, 11231-11238 (2005).

46 Huang, Z. L. *et al.* Adenosine A2A, but not A1, receptors mediate the arousal effect of caffeine. *Nat Neurosci* **8**, 858-859 (2005).

47 Alexandre, C. *et al.* Early life blockade of 5-hydroxytryptamine 1A receptors normalizes sleep and depression-like behavior in adult knock-out mice lacking the serotonin transporter. *J Neurosci* **26**, 5554-5564 (2006).

48 Anaclet, C. *et al.* Orexin/hypocretin and histamine: distinct roles in the control of wakefulness demonstrated using knock-out mouse models. *J Neurosci* **29**, 14423-14438 (2009).

49 Bjorness, T. E., Kelly, C. L., Gao, T., Poffenberger, V. & Greene, R. W. Control and function of the homeostatic sleep response by adenosine A1 receptors. *J Neurosci* **29**, 1267-1276 (2009).

50 He, Y. *et al.* The transcriptional repressor DEC2 regulates sleep length in mammals. *Science* **325**, 866-870 (2009).

1037 51 Qu, W. M. *et al.* Essential role of dopamine D2 receptor in the maintenance of
1038 wakefulness, but not in homeostatic regulation of sleep, in mice. *J Neurosci* **30**,
1039 4382-4389 (2010).

1040 52 Ma, T. *et al.* D-Serine Contributes to Seizure Development via ERK Signaling.
1041 *Front Neurosci* **13**, 254 (2019).

1042 53 Kashiwagi, M. *et al.* Widely Distributed Neurotensinergic Neurons in the
1043 Brainstem Regulate NREM Sleep in Mice. *Curr Biol* **30**, 1002-1010 (2020).

1044 54 Wang, J. H. & Desai, R. A brain protein and its effect on the Ca2+-and protein
1045 modulator-activated cyclic nucleotide phosphodiesterase. *Biochem Biophys Res*
1046 *Commun* **72**, 926-932 (1976).

1047 55 Watterson, D. M. & Vanaman, T. C. Affinity chromatography purification of a
1048 cyclic nucleotide phosphodiesterase using immobilized modulator protein, a
1049 troponin C-like protein from brain. *Biochem Biophys Res Commun* **73**, 40-46
1050 (1976).

1051 56 Klee, C. B. & Krinks, M. H. Purification of cyclic 3',5'-nucleotide
1052 phosphodiesterase inhibitory protein by affinity chromatography on activator
1053 protein coupled to Sepharose. *Biochemistry* **17**, 120-126 (1978).

1054 57 Klee, C. B., Crouch, T. H. & Krinks, M. H. Calcineurin: a calcium- and
1055 calmodulin-binding protein of the nervous system. *Proc Natl Acad Sci U S A* **76**,
1056 6270-6273 (1979).

1057 58 Stewart, A. A., Ingebritsen, T. S., Manalan, A., Klee, C. B. & Cohen, P. Discovery
1058 of a Ca2+- and calmodulin-dependent protein phosphatase: probable identity
1059 with calcineurin (CaM-BP80). *FEBS Lett* **137**, 80-84 (1982).

1060 59 Klee, C. B., Krinks, M. H., Manalan, A. S., Cohen, P. & Stewart, A. A. Isolation
1061 and characterization of bovine brain calcineurin: a calmodulin-stimulated protein
1062 phosphatase. *Methods Enzymol* **102**, 227-244 (1983).

1063 60 Cohen, P. & Cohen, P. T. Protein phosphatases come of age. *J Biol Chem* **264**,
1064 21435-21438 (1989).

1065 61 Guerini, D., Hubbard, M. J., Krinks, M. H. & Klee, C. B. Multiple forms of
1066 calcineurin, a brain isozyme of the calmodulin-stimulated protein phosphatase.
1067 *Adv Second Messenger Phosphoprotein Res* **24**, 242-247 (1990).

1068 62 Klee, C. B., Ren, H. & Wang, X. Regulation of the calmodulin-stimulated protein
1069 phosphatase, calcineurin. *J Biol Chem* **273**, 13367-13370 (1998).

1070 63 Mukai, H. *et al.* cDNA cloning of a novel testis-specific calcineurin B-like
1071 protein. *Biochem Biophys Res Commun* **179**, 1325-1330 (1991).

1072 64 Ueki, K., Muramatsu, T. & Kincaid, R. L. Structure and expression of two
1073 isoforms of the murine calmodulin-dependent protein phosphatase regulatory
1074 subunit (calcineurin B). *Biochem Biophys Res Commun* **187**, 537-543 (1992).

1075 65 Muramatsu, T. & Kincaid, R. L. Molecular cloning and chromosomal mapping
1076 of the human gene for the testis-specific catalytic subunit of calmodulin-
1077 dependent protein phosphatase (calcineurin A). *Biochem Biophys Res Commun*
1078 **188**, 265-271 (1992).

1079 66 Chang, C. D., Mukai, H., Kuno, T. & Tanaka, C. cDNA cloning of an alternatively
1080 spliced isoform of the regulatory subunit of Ca2+/calmodulin-dependent protein
1081 phosphatase (calcineurin B alpha 2). *Biochim Biophys Acta* **1217**, 174-180 (1994).

1082 67 Liu, L. *et al.* Characterization of a human regulatory subunit of protein
1083 phosphatase 3 gene (PPP3RL) expressed specifically in testis. *Mol Biol Rep* **32**,
1084 41-45 (2005).

1085 68 Miyata, H. *et al.* Sperm calcineurin inhibition prevents mouse fertility with
1086 implications for male contraceptive. *Science* **350**, 442-445 (2015).

1087 69 Liu, J. *et al.* Calcineurin is a common target of cyclophilin-cyclosporin A and
1088 FKBP-FK506 complexes. *Cell* **66**, 807-815 (1991).

1089 70 Rusnak, F. & Mertz, P. Calcineurin: form and function. *Physiol Rev* **80**, 1483-
1090 1521 (2000).

1091 71 Roy, J. & Cyert, M. S. Identifying New Substrates and Functions for an Old
1092 Enzyme: Calcineurin. *Cold Spring Harb Perspect Biol* **12**, a035436 (2020).

1093 72 Wigington, C. P. *et al.* Systematic Discovery of Short Linear Motifs Decodes
1094 Calcineurin Phosphatase Signaling. *Mol Cell* **79**, 342-358 (2020).

1095 73 Sonntag, T., Vaughan, J. M. & Montminy, M. 14-3-3 proteins mediate inhibitory
1096 effects of cAMP on salt-inducible kinases (SIKs). *FEBS J* **285**, 467-480 (2018).

1097 74 Daan, S., Beersma, D. G. & Borbely, A. A. Timing of human sleep: recovery
1098 process gated by a circadian pacemaker. *Am J Physiol* **246**, R161-183 (1984).

1099 75 Tobler, I. & Borbely, A. A. Sleep EEG in the rat as a function of prior waking.
1100 *Electroencephalogr Clin Neurophysiol* **64**, 74-76 (1986).

76 Suzuki, A., Sinton, C. M., Greene, R. W. & Yanagisawa, M. Behavioral and biochemical dissociation of arousal and homeostatic sleep need influenced by prior wakeful experience in mice. *Proc Natl Acad Sci U S A* **110**, 10288-10293 (2013).

77 Dijk, D. J., Beersma, D. G. & Daan, S. EEG power density during nap sleep: reflection of an hourglass measuring the duration of prior wakefulness. *J Biol Rhythms* **2**, 207-219 (1987).

78 Franken, P., Chollet, D. & Tafti, M. The homeostatic regulation of sleep need is under genetic control. *J Neurosci* **21**, 2610-2621 (2001).

79 Ai, H. W., Shen, W., Sagi, A., Chen, P. R. & Schultz, P. G. Probing protein-protein interactions with a genetically encoded photo-crosslinking amino acid. *Chembiochem* **12**, 1854-1857 (2011).

80 Suchanek, M., Radzikowska, A. & Thiele, C. Photo-leucine and photo-methionine allow identification of protein-protein interactions in living cells. *Nat Methods* **2**, 261-267 (2005).

81 Tanaka, Y., Bond, M. R. & Kohler, J. J. Photocrosslinkers illuminate interactions in living cells. *Mol Biosyst* **4**, 473-480 (2008).

82 Ash, C., Dubec, M., Donne, K. & Bashford, T. Effect of wavelength and beam width on penetration in light-tissue interaction using computational methods. *Lasers Med Sci* **32**, 1909-1918 (2017).

83 Luo, H. *et al.* Photocatalytic Chemical Crosslinking for Profiling RNA-Protein Interactions in Living Cells. *Angew Chem Int Ed Engl* **61**, e202202008 (2022).

84 Ngo, J. T. *et al.* Click-EM for imaging metabolically tagged nonprotein biomolecules. *Nat Chem Biol* **12**, 459-465 (2016).

85 Di Mascio, P. *et al.* Singlet Molecular Oxygen Reactions with Nucleic Acids, Lipids, and Proteins. *Chem Rev* **119**, 2043-2086 (2019).

86 Kolodziej, P. A. & Young, R. A. Epitope tagging and protein surveillance. *Methods Enzymol* **194**, 508-519 (1991).

87 Lizcano, J. M. *et al.* LKB1 is a master kinase that activates 13 kinases of the AMPK subfamily, including MARK/PAR-1. *EMBO J* **23**, 833-843 (2004).

88 Jaleel, M. *et al.* Identification of the sucrose non-fermenting related kinase SNRK, as a novel LKB1 substrate. *FEBS Lett* **579**, 1417-1423 (2005).

1133 89 Wang, Y. L., Wang, J., Chen, X., Wang, Z. X. & Wu, J. W. Crystal structure of
1134 the kinase and UBA domains of SNRK reveals a distinct UBA binding mode in
1135 the AMPK family. *Biochem Biophys Res Commun* **495**, 1-6 (2018).

1136 90 Cox, J., Pinto, L. & Dan, Y. Calcium imaging of sleep-wake related neuronal
1137 activity in the dorsal pons. *Nat Commun* **7**, 10763 (2016).

1138 91 Ding, F. *et al.* Changes in the composition of brain interstitial ions control the
1139 sleep-wake cycle. *Science* **352**, 550-555 (2016).

1140 92 Zhou, H. *et al.* Cholinergic modulation of hippocampal calcium activity across
1141 the sleep-wake cycle. *Elife* **8**, 39777 (2019).

1142 93 Niethard, N., Brodt, S. & Born, J. Cell-Type-Specific Dynamics of Calcium
1143 Activity in Cortical Circuits over the Course of Slow-Wave Sleep and Rapid Eye
1144 Movement Sleep. *J Neurosci* **41**, 4212-4222 (2021).

1145 94 Lee, J., Kim, D. & Shin, H. S. Lack of delta waves and sleep disturbances during
1146 non-rapid eye movement sleep in mice lacking alpha1G-subunit of T-type
1147 calcium channels. *Proc Natl Acad Sci U S A* **101**, 18195-18199 (2004).

1148 95 Yang, Z. Q. *et al.* Short-acting T-type calcium channel antagonists significantly
1149 modify sleep architecture in rodents. *ACS Med Chem Lett* **1**, 504-509 (2010).

1150 96 Astori, S. *et al.* The Ca(V)3.3 calcium channel is the major sleep spindle
1151 pacemaker in thalamus. *Proc Natl Acad Sci U S A* **108**, 13823-13828 (2011).

1152 97 Schneider, T. & Dibue-Adjei, M. Cav2.3 E-/R-type voltage-gated calcium
1153 channels modulate sleep in mice. *Sleep* **38**, 499 (2015).

1154 98 Jeghers, H., Mc, K. V. & Katz, K. H. Generalized intestinal polyposis and
1155 melanin spots of the oral mucosa, lips and digits; a syndrome of diagnostic
1156 significance. *N Engl J Med* **241**, 1031-1036 (1949).

1157 99 Peutz, J. L. A. Very remarkable case of familial polyposis of mucous membrane
1158 of intestinal tract and nasopharynx accompanied by peculiar pigmentations of
1159 skin and mucous membrane. *Nederl Maandschr Geneesk* **10**, 134-146 (1921).

1160 100 Hawley, S. A. *et al.* Complexes between the LKB1 tumor suppressor, STRAD
1161 alpha/beta and MO25 alpha/beta are upstream kinases in the AMP-activated
1162 protein kinase cascade. *J Biol* **2**, 28 (2003).

1163 101 Hong, S. P., Leiper, F. C., Woods, A., Carling, D. & Carlson, M. Activation of
1164 yeast Snf1 and mammalian AMP-activated protein kinase by upstream kinases.

Proc Natl Acad Sci U S A **100**, 8839-8843 (2003).

102 Sakamoto, K. *et al.* Deficiency of LKB1 in skeletal muscle prevents AMPK activation and glucose uptake during contraction. *EMBO J* **24**, 1810-1820 (2005).

103 Shaw, R. J. *et al.* The tumor suppressor LKB1 kinase directly activates AMP-activated kinase and regulates apoptosis in response to energy stress. *Proc Natl Acad Sci U S A* **101**, 3329-3335 (2004).

104 Shaw, R. J. *et al.* The kinase LKB1 mediates glucose homeostasis in liver and therapeutic effects of metformin. *Science* **310**, 1642-1646 (2005).

105 Sutherland, C. M. *et al.* Elm1p is one of three upstream kinases for the Saccharomyces cerevisiae SNF1 complex. *Curr Biol* **13**, 1299-1305 (2003).

106 Woods, A. *et al.* LKB1 is the upstream kinase in the AMP-activated protein kinase cascade. *Curr Biol* **13**, 2004-2008 (2003).

107 Liu, Y., Wang, T. V., Cui, Y., Gao, S. & Rao, Y. Biochemical purification uncovers mammalian sterile 3 (MST3) as a new protein kinase for multifunctional protein kinases AMPK and SIK3. *J Biol Chem* **298**, 101929 (2022).

108 Liu, Y. *et al.* STE20 phosphorylation of AMPK-related kinases revealed by biochemical purifications combined with genetics. *J Biol Chem* **298**, 101928 (2022).

109 Platt, R. J. *et al.* CRISPR-Cas9 knockin mice for genome editing and cancer modeling. *Cell* **159**, 440-455 (2014).

110 Sunagawa, G. A. *et al.* Mammalian Reverse Genetics without Crossing Reveals Nr3a as a Short-Sleeper Gene. *Cell Rep* **14**, 662-677 (2016).

111 Yardeni, T., Eckhaus, M., Morris, H. D., Huizing, M. & Hoogstraten-Miller, S. Retro-orbital injections in mice. *Lab Anim (NY)* **40**, 155-160 (2011).

112 Barger, Z., Frye, C. G., Liu, D., Dan, Y. & Bouchard, K. E. Robust, automated sleep scoring by a compact neural network with distributional shift correction. *PLoS One* **14**, e0224642 (2019).

FIGURE LEGENDS

Fig. 1| Sleep phenotype of T469A mutant male mice. Sleep phenotype of male mice with either SIK3$^{+/+}$ genotype or SIK3$^{T469A/+}$ genotype. SIK3$^{T469A/\ T469A}$ males were embryonic lethal although females of all three genotypes including SIK3$^{T469A/\ T469A}$ were viable and analyzed in Extended Data Figs. 3 and 4. For detailed numbers, see Extended Data Tables 1 and 2. **a, b**, profiles showing sleep time each hour in min/hr (**a**) or profiles of NREM sleep (**b**). The x axis shows zeitgeber time (ZT) with the white box indicating light phase (or daytime) and black box dark phase (or nighttime). The black line shows data from SIK3$^{+/+}$ mice (n = 11), the blue line data from SIK3$^{T469A/+}$ mice (n = 10). ns: statistically not significant. *p<0.05; **p<0.01; mean ± standard error of the mean (SEM) (Two-way ANOVA with Tukey's multiple comparisons test). **c,d,** Data and statistics of NREM sleep duration (**c,** *p< 0.05, **p<0.01; ns, not significant; mean ± SEM, One-way ANOVA with Tukey's multiple comparisons test), NREM sleep episode number (**d**, ns, not significant; mean ± SEM, Kruskal-Wallis test with Dunn's multiple comparisons test), and NREM sleep episode duration (**e**, ns, not significant; mean ± SEM, Kruskal-Wallis test with Dunn's multiple comparisons test). **f**, EEG power spectrum during NREM sleep. X-axis indicates frequency distribution of EEG power. *p<0.05; mean ± SEM (Two-way repeated measurement ANOVA with Tukey's multiple comparisons test). **g**, Diurnal NREMS delta density. *p<0.05; **p<0.01; ***p<0.001; ns, not significant; mean ± SEM (Mixed-effects model)

NREMS delta power density over 24 hours. X-axis indicates ZT. **h**, Probabilities of transition between different sleep and wake states. ns, not significant; mean ± SEM (Two-way ANOVA with Tukey's multiple comparisons test). **i**, Recovery of NREM sleep after 6 hrs of SD. ns, not significant; mean±SEM (Two-way repeated measurement ANOVA with Tukey's multiple comparisons test). **j**, One hr representative EEG and EMG graphs at different vigilance states (wake, NREM, REM).

Fig. 2| Biochemical purification of SIK3 phosphatases from HEK cells. a, 500 mg (at a concentration of 10 mg/ml) of HEK cell lysates was fractionated on a QHP column, eluted with a linear gradient of NaCl (0-600 mM) and the final wash with 1 M NaCl buffer A. Each fraction was dialyzed into buffer A, removing NaCl. 10 µl of each sample was used for analysis of activities removing phosphate from SIK3 T469 and S551. T469 and S551 of bacterially expressed recombinant SIK3 were phosphorylated by PKA in vitro before being used to test phosphatase activities of the fractions of HEK lysates. Fractions 10 to 13 contained significant activities removing phosphate from SIK3 T469 and S551. **b**, Fractions 10 to 13 from QHP were combined and dialyzed with buffer A before being loaded onto a Blue HP column. It was eluted with a linear gradient of NaCl (0-600 mM) and the final wash with 1 M NaCl buffer A. The flow through (FL) fraction from the Blue HP contained significant activities removing phosphate from SIK3 T469 and S551. **c,** The FL fraction from

the Blue HP column was dialyzed with buffer A and loaded onto a SP-HP column. The fractionation was similar to those in (**a**) and (**b**). The FL fraction from the SP-HP column contained significant activities removing phosphate from SIK3 T469 and S551. **d,** The FL fraction from the SP-HP column was dialyzed with buffer A and loaded onto a heparin column. The rest of the fractionation was similar to (**a**) and (**b**). The FL fraction and fraction 1 contained significant activities removing phosphate from SIK3 T469 and S551. **e,** The FL fraction from the heparin column was dialyzed with buffer A and loaded onto a HAP-HP column. The rest of the fractionation was similar to (**a**) and (**b**) except that the final wash was with 5 CVs of 500 mM K_2PO_4. Fractions 5 to 7 contained significant activities removing phosphate from SIK3 T469 and S551. **f,** Active fractions from the HAP-HP column were condensed into 0.5 ml, fractionated on a Superdex 200 molecular sieve column, eluted with 300 mM NaCl gradient into 20 CVs. 1 ml from each fraction was collected and labeled as samples 1 to 20. Protein contents were monitored with UV at 280 nm.

Fig. 3| Identification of protein phosphatases purified from HEK cells. a, A schematic illustration of phosphatase purification with HEK cell lysates passing through Q HP, Blue HP, SP HP, heparin HP, HAP HP and Superdex 200 columns before silver staining and mass spectroscopic analysis. **b,** Fractions from the Superdex 200 column with strongest phosphatase activities for T469 and S551 in Fraction 15. 25 µl of each fraction (from Fraction 10 to Fraction 18) was run onto a

gel and silver-stained. The thick band indicated by the arrow was analyzed by mass spectroscopy. **c,** 4 protein phosphatases were found by MS.

Fig. 4| Proteins interacting with SIK3 identified by photo-crosslinking. a, A schematic diagram of our newly invented photo crosslinking method (RG and PC) (for details, see the method section). We have generated a mouse line with the SIK3 tagged at its C terminus with 3 repeats of the HA epitope. Brain slices were prepared from SIK3-HA mice and photocatalytic crosslinking was carried out in darkness with eosin Y (50 μM) and 1, 6 dihexamine (1 mM). The anti-HA antibody was used to pull down proteins crosslinked to SIK3. **b,** Comparison of proteins pulled down by anti-HA before and after light treatment. Validation of photocatalytic crosslinking efficacy in mouse brain slices. 1 hr green light was given after photocatalytic reagents treatment and slices were collected and homogenized. The arrowhead indicates SIK3-interaction proteins. **c**-**d**, Veen (**c**) and volcano (**d**) plot of putative SIK3 interaction proteins enriched in photo-linkage groups. The red dot is PPP3CA. **e**-**f**, Co-immunoprecipitation between PPP3CA and SIK3 from WT mouse brain homogenates using anti-SIK3 and anti-PPP3CA antibodies. **g**-**h,** Co-immunoprecipitation between the HA tagged PPP3CA and FLAG tagged SIK3 in HEK293T cells using anti-FLAG and anti-HA antibodies. HEK293T cells were co-overexpressed with 1 μg HA-PPP3CA and 1 μg FLAG-SIK3 expressing plasmids for 24 hrs before cell collection and lysis.

Fig. 5| Site-specific dephosphorylation of SIK3 by PPP3CA in vitro. a, PPP3CA, PPP3CB, PPP3CC and PPP5C were individually tagged with FLAG and transfected into HEK 293T cells. PPP3R1 was also separately transfected into HEK 293T cells. SIK3-FLAG was transfected into HEK 293T cells. Each of the PPases and the regulatory PPP3R1 was separately immunoprecipitated by the anti-FLAG antibody from HEK cells. Under the same conditions (in the presence of PPP3R1), PPP3CA, PPP3CB or PPP3CC could dephosphorylate SIK3 at T469 and S551, but not T221. PPP5C could no dephosphorylate SIK3 at T469, S551or T221.**b-e,** In the presence of PPP3R1 immunoprecipitated from HEK cells, increasing concentrations (from + to +++) of PPP3CA immunoprecipitated from HEK cells could not dephosphorylate AKT1 at T308, PDK1 at S241, MARK1 at T215, GSK3β at S9, JNK1 at T183, ERK2 at T185. In the presence of PPP3R1 immunoprecipitated from HEK cells, PPP3CA immunoprecipitated from HEK cells could dephosphorylate MEK1 at S217 (**b**). **f,** Recombinant PPP3CA, PPP3R1, CaM were expressed in and purified from *E. coli*. Full-length SIK3 was immunoprecipitated from HEK 293T cells. In the presence of Ca^{2+}, PPP3R1 and CaM, PPP3CA dephosphorylated SIK3 at T469 or S551but not at T221.

Fig. 6| SIK3 dephosphorylation and PPP3CA in HEK cells. a-b, Ionomycin dephosphorylated SIK3 at T469 and S551 (but not T221) in a dose-(**a**) and time- (**b**)

dependent manner. **c**, Transfection of increasing dosage of PPP3CA and PPP3R1 into HEK cells enhanced the dephosphorylation response of SIK3-T469 and SIK3-S551 to ionomycin. In the absence of ionomycin, increasing the dosages of PPP3CA and PPP3R1 alone did not significantly changed SIK3-T469 and SIK3-S551 phosphorylation. After transfection for 24 hrs, cells were treated with 10 μg/ml ionomycin for 10 min. **d**, Transfection of a catalytically inactive PPP3CA mutant (H151A) and PPP3R1 into HEK cells did not enhance the dephosphorylation response of SIK3-T469 and SIK3-S551 to ionomycin. **e,** Transfection of sgRNA targeting GFP into HEK 293T cells did not significantly affect the dephosphorylation response of SIK3-T469 and SIK3-S551 to ionomycin. Transfection of sgRNA targeting either PPP3CA or PPP3CB alone into HEK 293T cells affected the dephosphorylation response of SIK3-T469 and SIK3-S551 to ionomycin in a variable manner (data not shown). Transfection of sgRNAs targeting both PPP3CA and PPP3CB into HEK 293T cells robustly and significantly reduced the dephosphorylation response of SIK3-T469 and SIK3-S551 to ionomycin. Transfection of sgRNA targeting PPP3R1 into HEK 293T cells robustly and significantly reduced the dephosphorylation response of SIK3-T469 and SIK3-S551 to ionomycin. PPP3R1 targeting reduced the protein levels of itself as well as PPP3CA, and PPP3CB in HEK cells. PPP3CA and PPP3CB targeting reduced the protein levels of themselves as well as PPP3R1 in HEK cells, indicating the inter-dependence of CaN catalytic and regulatory subunits.

Fig. 7| Serine/threonine phosphorylation in the mouse brain after PPP3CA or PPP3R1 knockdown. Phosphorylation of different proteins was examined by anti-phospho-protein antibodies. Each lane shows results from one mouse, and three from each genotype are shown individually here to allow visualization of consistency. **a,** From the left are: two WT mice injected with sgRNAs targeting GFP, five CAS9 expressing mice injected with sgRNAs targeting GFP, and five CAS9 expressing mice injected with sgRNAs targeting PPP3CA. Phosphorylation of SIK3 T469 and SIK3 S551 was reproducibly increased in mice only when sgRNAs targeting PPP3CA were injected into CAS9 expressing mice, neither the WT mice nor with sgRNAs targeting GFP. Phosphorylation of SIK3 T221 did not change. AMPK-T172 phosphorylation was variable in each mouse, not dependent on the expression of CAS9 or sgRNAs targeting PPP3CA. **b,** From the left are: three WT mice injected with sgRNAs targeting GFP, three CAS9 expressing mice injected with sgRNAs targeting GFP, and three CAS9 expressing mice injected with sgRNAs targeting PPP3R1. Phosphorylation of SIK3 T469 and SIK3 S551 was reproducibly increased in mice only when sgRNAs targeting PPP3R1 were injected into CAS9 expressing mice, neither the WT mice nor with sgRNAs targeting GFP. Phosphorylation of SIK3 T221 did not change. AMPK-T172 phosphorylation was variable in each mouse, not dependent on the expression of CAS9 or sgRNAs targeting PPP3R1.

Fig. 8| Sleep phenotype of mice after PPP3CA knockdown. Sleep phenotypes of male mice with the genotypes of $PPP3CA^{KD}$ (red, n=21), $eGFP^{Ctrl}$ (black, n=18) and WT^{Ctrl} mice (blue, n=12). $PPP3CA^{KD}$ denotes $Rosa26^{Cas9/+}$ mice injected with AAV-PPP3CA-sgRNA virus; $eGFP^{Ctrl}$ denotes $Rosa26^{Cas9/+}$ mice injected with AAV-eGFP-sgRNA virus; WT^{Ctrl} denotes WT littermate mice injected with AAV-PPP3CA-sgRNA virus. For detailed numbers, see also Extended Data Tables 3 and 4. **a-b,** profiles of sleep (**a**) or NREM (**b**). *p< 0.05; ****p<0.0001; ns, not significant; mean±SEM (Two-way ANOVA with Tukey's multiple comparisons test). **c,** Data and statistics of NREM sleep over 24 hrs. *p< 0.05, ****p<0.0001; ns, not significant; mean ± SEM (One-way ANOVA with Tukey's multiple comparisons test). **d-e**, NREM sleep episode number (**d**) and NREM sleep episode duration of (**e**). *p<0.05; **p<0.01; ***p<0.001; ****p<0.0001; ns, not significant; mean±SEM (Kruskal-Wallis test with Dunn's multiple comparisons test). **f,** EEG power spectrum during NREM sleep. *p < 0.05; mean ± SEM (Two-way repeated measurement ANOVA with Tukey's multiple comparisons test). **g,** NREMS delta densities over 14 hrs. X-axis indicates ZT. Data at ZT13 was not included in statistical analysis due to the inaccessible values from $PPP3CA^{KD}$ mice. *p<0.05; **p<0.01; ***p<0.001; ns, not significant; mean±SEM (Mixed-effects model). **h,** Probabilities of transition between different sleep and wake states. *p<0.05; **p<0.01; ***p<0.001; ****p<0.0001; ns, not significant; mean±SEM (Two-way ANOVA with Tukey's multiple comparisons test). **i,** A diagram illustrating probabilities of transition between different sleep and wke states. **j,**

Recovery of NREM sleep after 6 hrs of SD. *p<0.05; **p<0.01; ***p<0.001; ****p<0.0001; ns, not significant; mean±SEM (Two-way repeated measurement ANOVA with Tukey's multiple comparisons test). **k,** One hr representative EEG and EMG graphs at different vigilance states.

Fig. 9| Sleep phenotype of mice after PPP3R1 knockdown. Sleep phenotypes of male mice with the genotypes of $PPP3R1^{KD}$ (red, n=11), $eGFP^{Ctrl}$ (black, n=11) and WT^{Ctrl} mice (blue, n=14). $eGFP^{Ctrl}$: $Rosa26^{Cas9/+}$ mice injected with AAV-eGFP-sgRNA virus. WT^{Ctrl}: WT mice injected with AAV-PPP3R1-sgRNA virus. $PPP3R1^{KD}$: $Rosa26^{Cas9/+}$ mice injected with AAV-PPP3R1-sgRNA virus. For details, see also Extended Data Tables 5 and 6. **a-b,** Sleep profiles (**a**) or profiles of NREM sleep (**b**). ns: statistically not significant; ****p<0.0001; mean ± SEM (Two-way ANOVA with Tukey's multiple comparisons test). **c,** Data and statistics of NREM sleep over 24 hrs. ns: statistically not significant; *p< 0.05; ****p<0.0001; mean ± SEM (One-way ANOVA with Tukey's multiple comparisons test). **d-e,** NREM sleep episode number (**d**), and NREM sleep episode duration (**e**). ns: statistically not significant; *p< 0.05; **p<0.01; ***p<0.001; ****p<0.0001; mean ± SEM (Kruskal-Wallis test with Dunn's multiple comparisons test). **f,** NREMS EEG power spectrum analysis. X-axis indicates frequency distribution of EEG power. *p<0.05; mean ± SEM (Two-way repeated measurement ANOVA with Tukey's multiple comparisons test). **g,** NREMS delta power density over 24 hours. X-axis indicates ZT. Statistical analysis each hr

shown in *s. ns: statistically not significant; *p< 0.05; **p<0.01; ***p<0.001; ****p<0.0001; mean ± SEM (Mixed-effects model). **h,** Transition probabilities of different sleep and wake states. W: wake, NR: NREM Sleep, R: REM Sleep. ns: statistically not significant; *p< 0.05; **p<0.01; ***p<0.001; ****p<0.0001; mean ± SEM (Two-way ANOVA with Tukey's multiple comparisons test). **i,** A diagrammatic illustration of transition probabilities of different sleep and wake states, summarized from data in Fig. 9H and Fig. S9K and S9L. ns: no significant changes. **j,** Cumulative NREMS rebound after 6 hrs of SD. ns: statistically not significant; *p< 0.05; **p<0.01; ***p<0.001; ****p<0.0001; mean ± SEM (Two-way repeated measurement ANOVA with Tukey's multiple comparisons test). **k,** Representative one hour EEG and EMG signals.

Legends for Extended Data Figures and Tables

Extended Data Fig. 1| Additional sleep phenotype of male T469A mutant mice. a-d, Profiles of wake over 24 hrs (**a**), total wake duration over 24 hrs (**b**), wake episode number (**c**), wake episode duration (**d**) of $SIK3^{T469A/+}$ (blue, n=10) and $SIK3^{+/+}$ mice (black, n=11). *p<0.05; ns, not significant; mean±SEM (A: Two-way ANOVA with Tukey's Multiple comparisons test; B: One-way ANOVA with Tukey's multiple comparisons test; C-D: Kruskal-Wallis test with Dunn’s multiple comparisons test). **e-h,** Profiles of REM sleep over 24 hrs (**e**), total REM duration over 24 hrs (**f**), REM episode number (**g**), REM episode duration (**h**). *p<0.05; ns, not significant; mean ±

SEM (E: Two-way ANOVA with Tukey's multiple comparisons test; F: One-way ANOVA with Tukey's multiple comparisons test; G-H: Kruskal-Wallis test with Dunn's multiple comparisons test). **i-j,** EEG power spectrum during wake (**i**) or REM sleep (**j**). *p<0.05; mean±SEM (Two-way repeated measurement ANOVA with Tukey's multiple comparisons test). **k-l,** Probabilities of transition between different sleep and wake states.

Extended Data Fig. 2| Additional sleep phenotype of Male T469A mutant mice. **a-b,** Recovery of wake (**a**) or REM sleep (**b**) after 6 hrs of SD. *p< 0.05; **p<0.01; ****p<0.0001; ns, not significant; mean ± SEM (Two-way ANOVA with Tukey's multiple comparisons test). **c,** NREMS delta densities during the 24 hr recovery after SD. *p< 0.05; **p <0.01; ***p<0.001; ****p <0.0001; ns, not significant; mean ± SEM (Mixed-effects model). **d,** Changes of NREM delta power densities after SD. ns, not significant; mean ± SEM (Two-way repeated measurement ANOVA with Tukey's multiple comparisons test). **e,** Representative hypnograms.

Extended Data Fig. 3| Sleep phenotype of female T469A mutant mice. Unlike males for which we could not obtain $SIK3^{T469A/T469A}$ mutants, we did obtain all three genotypes for female mice: $SIK3^{T469A/T469A}$ (red, n=5), $SIK3^{T469A/+}$ (blue, n=6) and $SIK3^{+/+}$ (black, n=7). **a-d,** Profiles of NREM over 24 hrs (**A**), total NREM duration over 24 hrs (**b**), NREM episode number (**c**), NREM episode duration (**d**). *p<0.05; ns,

not significant; mean ± SEM (**a**: Two-way ANOVA with Tukey's multiple comparisons test; **b**: One-way ANOVA with Tukey's multiple comparisons test; **c**-**d**: Kruskal-Wallis test with Dunn's multiple comparisons test). **e-h,** Profiles of REM sleep over 24 hrs (**e**), total REM duration over 24 hrs (**f**), REM episode number (**g**), REM episode duration (**h**). *p<0.05; **p <0.01; ns, not significant; mean ± SEM (**e**: Two-way ANOVA with Tukey's multiple comparisons test; **f**: One-way ANOVA with Tukey's multiple comparisons test; **g-h**: Kruskal-Wallis test with Dunn's multiple comparisons test). **i-l,** Profiles of wake over 24 hrs (**i**), total wake duration over 24 hrs (**j**), wake episode number (**k**), wake episode duration (**l**). *p<0.05; ns, not significant; mean±SEM (**i**: Two-way ANOVA with Tukey's multiple comparisons test; **j**: One-wayANOVA with Tukey's multiple comparisons test; **k**-**l**: Kruskal-Wallis test with Dunn's multiple comparisons test). **m-p,** Probabilities of transition between different sleep and wake states. *p<0.05; **p<0.01; ***p<0.001; ****p<0.0001; ns, not significant; mean±SEM (Two-way ANOVA with Tukey's multiple comparisons test).

Extended Data Fig. 4| Additional sleep phenotype of female T469A mutant mice. **a-c,** EEG power spectrum during NREM sleep (**a**), REM sleep (**b**) or wake (**c**). *p< 0.05; mean ± SEM (Two-way repeated measurement ANOVA with Tukey's multiple comparisons test). **d,** Diurnal NREM delta power densities. *p<0.05; **p<0.01; ***p<0.001; ****p<0.0001; ns, not significant; mean±SEM (Mixed-effects model). **e**-**g**, Recovery of NREM (**e**), REM (**f**) and wake (**g**) after 6 hrs of SD. ns, not significant;

mean±SEM (Two-way ANOVA with Tukey's multiple comparisons test). **h,** NREMS delta densities during the 24 hr recovery time. *p<0.05; **p<0.01; ***p<0.001; ****p <0.0001; ns, not significant; mean ± SEM (Mixed-effects model). **i,** Changes of NREM delta densities after 6 hrs of SD. *p< 0.05; **p<0.01; ns, not significant; mean±SEM (Two-way repeated measurement ANOVA with Tukey's multiple comparisons test). **j,** One hr representative EEG and EMG signals of littermates at each vigilance state. **k,** Representative hypnograms.

Extended Data Fig. 5| Specificities of antibodies against SIK3 T469 and SIK3 S551 phosphorylated by PKA. Recombinant SIK3 fragment containing its amino acid residues 1 to 558 was expressed in and purified from *E. coli* before being treated by PKA in the presence of ATP. The PKA used was a mutant (PKA^{T197E}) expressed in and purified from *E. coli*. Recombinant PKA^{T197E} phosphorylated SIK3 at T469 and S551, but not T221. Anti-phospho-$SIK3^{T469}$ and anti-phospho-$SIK3^{S551}$ antibodies specifically recognized T469 and S551, but not T221, of SIK3 under the same conditions.

Extended Data Fig. 6| A schematic diagram of virally mediated gene knockdown in mice. A host mouse either was WT or could express CAS9 from its Rosa26 site ($Rosa26^{Cas9/+}$) and was injected with an AAV virus two weeks before an EEG recorder was placed on its head.

Extended Data Fig. 7| Additional sleep phenotype of male PPP3CA knockdown mice. a-d, Profiles of wake over 24 hrs (**a**), total wake duration over 24 hrs (**b**), wake episode number (**c**), wake episode duration (**d**). Wake was increased by approximately 3 hrs in PPP3CA^{KD} mice as compared to either control. Wake was increased during daytime by approximately 80 mins, due to increased wake episode duration (Extended Fig. 7d) albeit decreased wake episode number (Extended Data Fig. 7c) in PPP3CA^{KD} mice. Wake was significantly increased in nighttime by approximately 100 mins (Extended Data Fig. 7 a-b), due to increased duration (Extended Data Fig. 7d) albeit decreased number (Extended Data Fig. 7c) of wake episodes. *p<0.05; **p<0.01; ***p<0.001; ****p<0.0001; ns, not significant; mean±SEM (**a**: Two-way ANOVA with Tukey's multiple comparisons test; **b**: One-way ANOVA with Tukey's multiple comparisons test; **c-d**: Kruskal-Wallis test with Dunn's multiple comparisons test. **e-h,** Profiles of REM sleep over 24 hrs (**e**), total REM duration over 24 hrs (**f**), REM episode number (**g**), REM episode duration (**h**). *p< 0.05; **p<0.01; ***p<0.001; ****p<0.0001; ns, not significant; mean±SEM (**e**: Two-way ANOVA with Tukey's multiple comparisons test; **f**: One-way ANOVA with Tukey's multiple comparisons test; **g-j**: Kruskal-Wallis test with Dunn's multiple comparisons test). **i-j,** EEG power spectrum during wake and REM sleep. *p< 0.05; mean ± SEM (Two-way repeated measurement ANOVA with Tukey's multiple comparisons test). **k-l,** Probabilities of transition between different sleep and wake states. *p< 0.05, **p<0.01, ***p<0.001

and ****p<0.0001, mean±SEM. (Two-way repeated measurement ANOVA with Tukey's multiple comparisons test).

Extended Data Fig. 8| Additional sleep phenotype of male PPP3CA knockdown mice. a-b, Recovery of wake (**a**) and REM sleep (**b**) after 6 hrs of SD. *p< 0.05; **p <0.01; ***p<0.001; ****p<0.0001; ns, not significant; mean±SEM (Two-way ANOVA with Tukey's multiple comparisons test). **c,** NREMS delta densities during the 24 hr recovery time. *p< 0.05; **p<0.01; ns, not significant; mean±SEM (Mixed-effects model). **d,** Changes of NREM delta densities after 6 hrs of SD. *p< 0.05; ns, not significant; mean±SEM (Two-way repeated measurement ANOVA with Tukey's multiple comparisons test). **e,** Representative hypnograms.

Extended Data Fig. 9| Additional sleep phenotype of PPP3R1 knockdown male mice. a-d, Wake analysis: profiles showing wake time each hour in mins/hr with the X axis indicating ZT (**a**), total wake time over 24 hrs, wake time during the light phase (daytime) or the dark phase (**b**), wake episode number (**c**), wake episode duration (**d**). ns: statistically not significant; *p< 0.05; **p<0.01; ***p<0.001; ****p<0.0001; mean±SEM (a: Two-way ANOVA with Tukey's multiple comparisons test; b: One-way ANOVA with Tukey's multiple comparisons test; c-d: Kruskal-Wallis test with Dunn’s multiple comparisons test). **e-h,** REM analysis: profiles showing REM duration each hour in mins/hr with the X axis indicating ZT (**e**), total REM time over

24 hrs, REM time during the light phase (daytime) or the dark phase (**f**), REM episode number (**g**), REM episode duration (**h**). ns: statistically not significant; *p< 0.05; **p<0.01; ***p<0.001; ****p<0.0001; mean±SEM (**e**: Two-way ANOVA with Tukey's multiple comparisons test; **f**: One-way ANOVA with Tukey's multiple comparisons test; **g**-**h**: Kruskal-Wallis test with Dunn's multiple comparisons test). (**i**-**j**) EEG power spectrum analysis of wake (**i**) and REM sleep (**j**). *p<0.05; mean±SEM (Two-way repeated measurement ANOVA with Tukey's multiple comparisons test). **k-l,** Transition probabilities of different sleep and wake states. ns: statistically not significant; *p< 0.05; **p<0.01; ***p<0.001; ****p<0.0001; mean±SEM. (Two-way repeated measurement ANOVA with Tukey's multiple comparisons test).

Extended Data Fig. 10| Additional sleep phenotype of PPP3R1 knockdown male mice. a-b, Recovery of umulative wake (**a**) and REMS b) after 6 hrs of SD. ns: statistically not significant; *p< 0.05; **p<0.01; ***p<0.001; ****p<0.0001; mean±SEM (Two-way ANOVA with Tukey's multiple comparisons test). **c,** NREM delta power densities during the 24 hr recovery period after 6 hrs of SD. ns: statistically not significant; *p< 0.05; **p<0.01; ***p<0.001; ****p<0.0001;mean±SEM (Mixed-effects model). **d,** Changes of NREM delta power densities between pre- and post-SD. ns: statistically not significant; *p< 0.05; **p<0.01; ***p<0.001; ****p<0.0001;

mean±SEM (Two-way repeated measurement ANOVA with Tukey's multiple comparisons test). **e,** Representative hypnograms.

Extended Data Table 1| Total Time spent in different sleep-wake states by SIK3$^{+/+}$, SIK3$^{+/T469A}$ and SIK3 $^{T469A /T469A}$ mice.

Extended Data Table 2| Differences in total time spent in different sleep-wake states by SIK3$^{+/+}$, SIK3$^{+/T469A}$ and SIK3 $^{T469A /T469A}$ Mice.

Extended Data Table 3| Total time spent in different sleep-wake States by eGFP^{Ctrl}, WT^{Ctrl} and PPP3CA^{KD} mice.

Extended Data Table 4| Differences in total time spent in different sleep-wake states by eGFP^{Ctrl}, WT^{Ctrl} and PPP3CA^{KD} ,ice.

Extended Data Table 5| Total time spent in different sleep-wake states by eGFP^{Ctrl}, WT^{Ctrl} and PPP3R1^{KD} mice.

Extended Data Table 6| Differences in total time spent in different sleep-wake states by eGFP^{Ctrl}, WT^{Ctrl} and PPP3R1^{KD} mice.

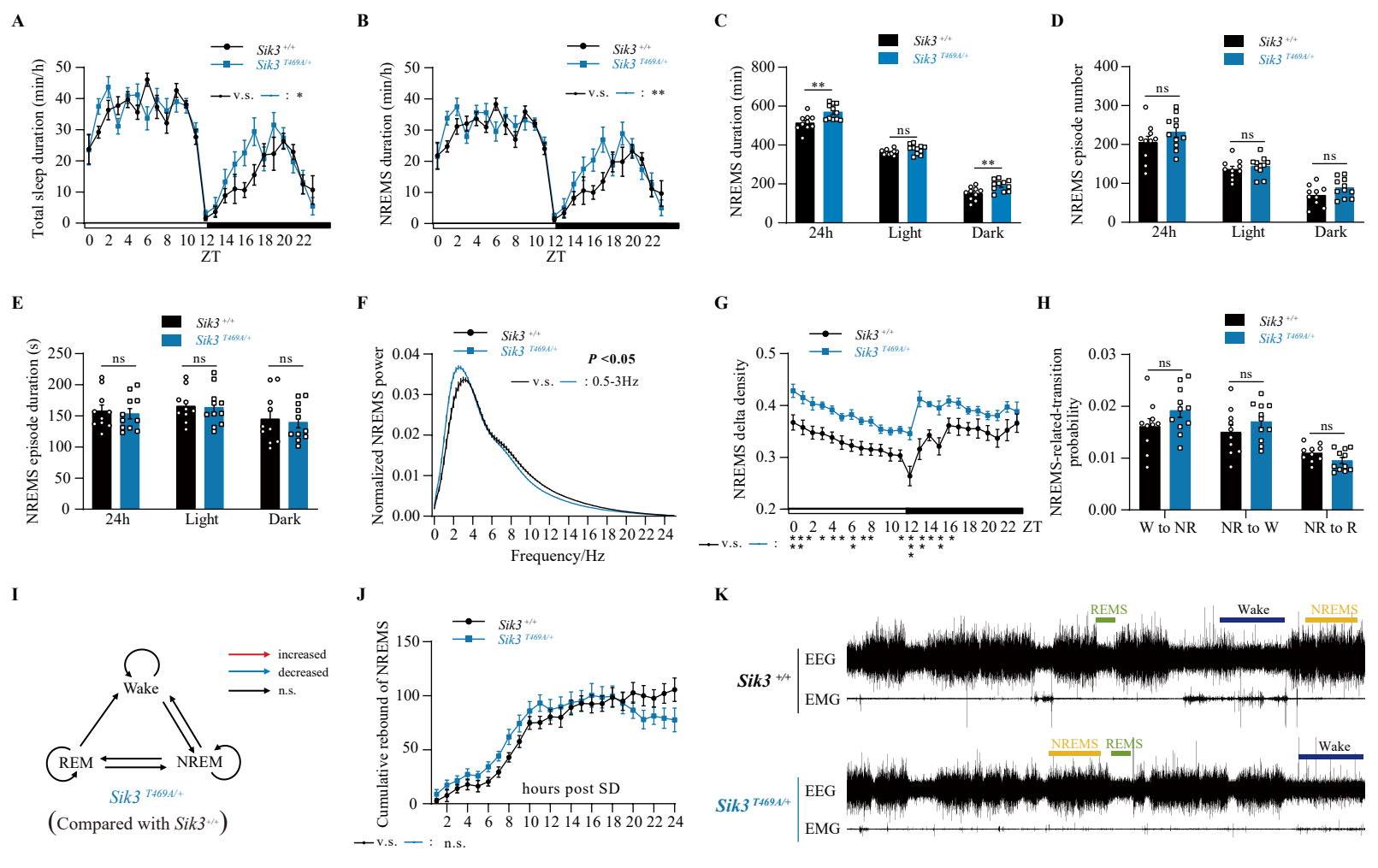
A
Total sleep duration (min/h)
Sik3 +/+
Sik3 T469A/+
v.s. : *
ZT
B
NREMS duration (min/h)
v.s. : **
C
NREMS duration (min)
24h
Light
Dark
D
NREMS episode number
ns
E
NREMS episode duration (s)
F
Normalized NREMS power
P <0.05
v.s. : 0.5-3Hz
Frequency/Hz
G
NREMS delta density
H
NREMS-related-transition probability
W to NR
NR to W
NR to R
I
Wake
REM
NREM
increased
decreased
n.s.
Sik3 T469A/+
(Compared with Sik3+/+)
J
Cumulative rebound of NREMS
hours post SD
K
REMS
Wake
NREMS
EEG
EMG

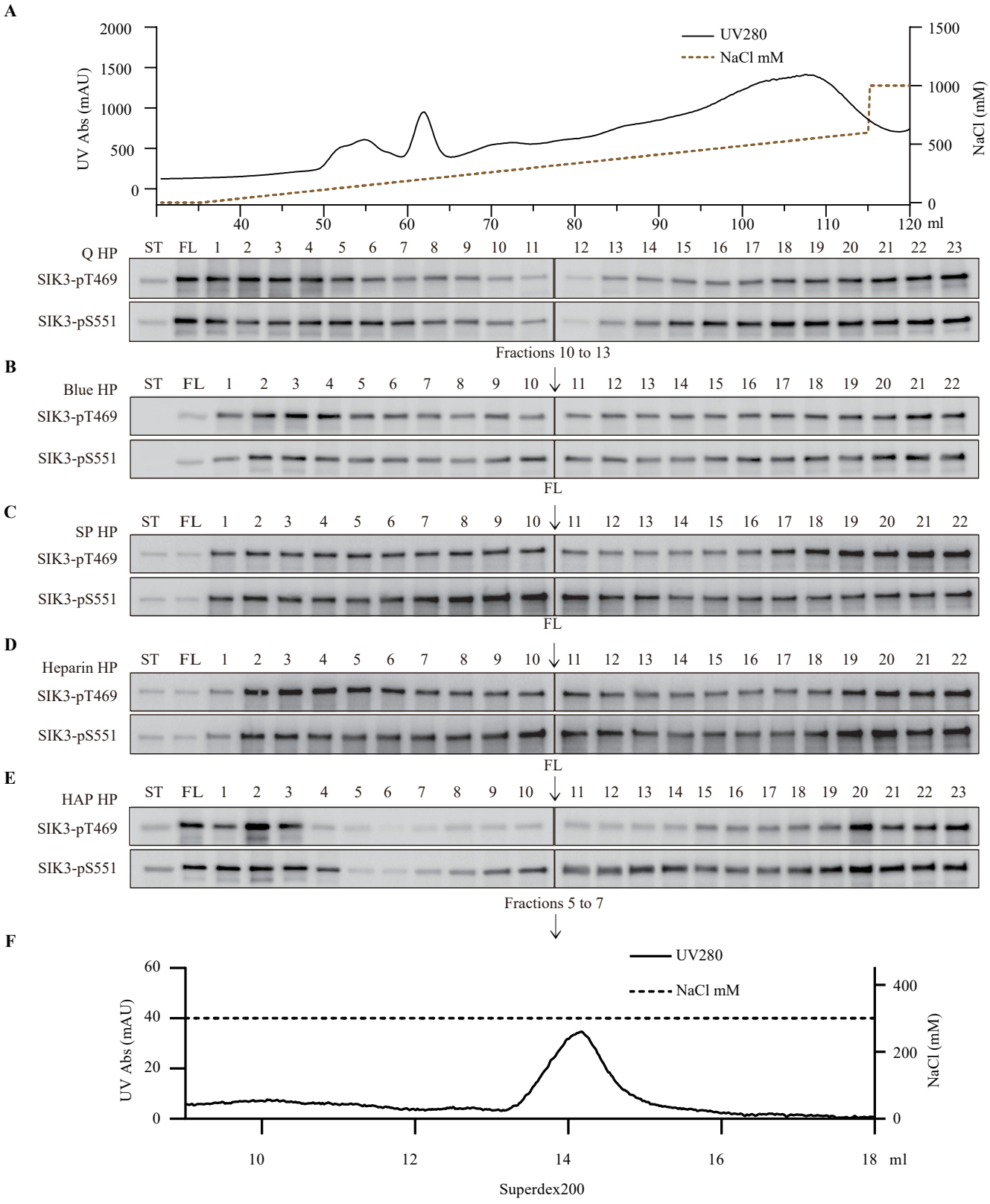
A
UV280
NaCl mM
UV Abs (mAU)
NaCl (mM)
ml
Q HP
ST FL 1 2 3 4 5 6 7 8 9 10 11 12 13 14 15 16 17 18 19 20 21 22 23
SIK3-pT469
SIK3-pS551
Fractions 10 to 13
B
Blue HP
ST FL 1 2 3 4 5 6 7 8 9 10 11 12 13 14 15 16 17 18 19 20 21 22
SIK3-pT469
SIK3-pS551
FL
C
SP HP
ST FL 1 2 3 4 5 6 7 8 9 10 11 12 13 14 15 16 17 18 19 20 21 22
SIK3-pT469
SIK3-pS551
FL
D
Heparin HP
ST FL 1 2 3 4 5 6 7 8 9 10 11 12 13 14 15 16 17 18 19 20 21 22
SIK3-pT469
SIK3-pS551
FL
E
HAP HP
ST FL 1 2 3 4 5 6 7 8 9 10 11 12 13 14 15 16 17 18 19 20 21 22 23
SIK3-pT469
SIK3-pS551
Fractions 5 to 7
F
UV280
NaCl mM
UV Abs (mAU)
NaCl (mM)
ml
Superdex200

A

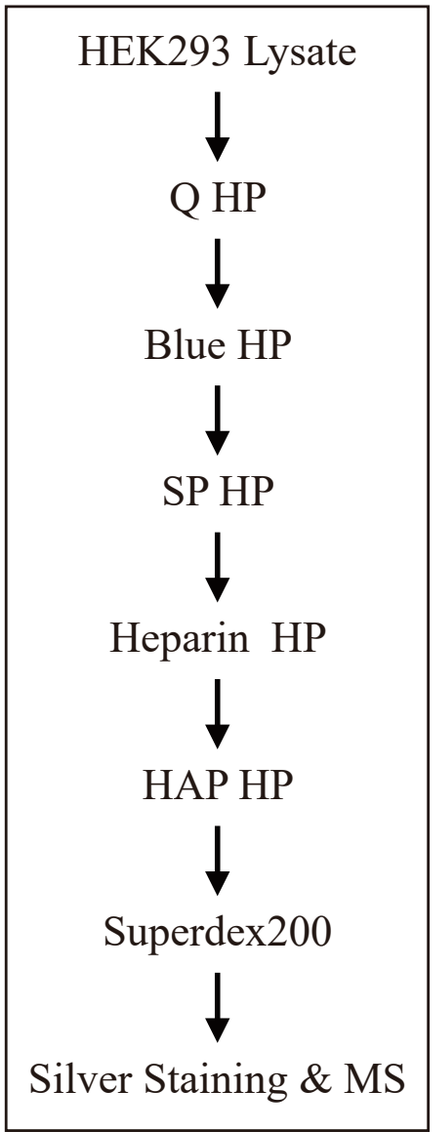

B

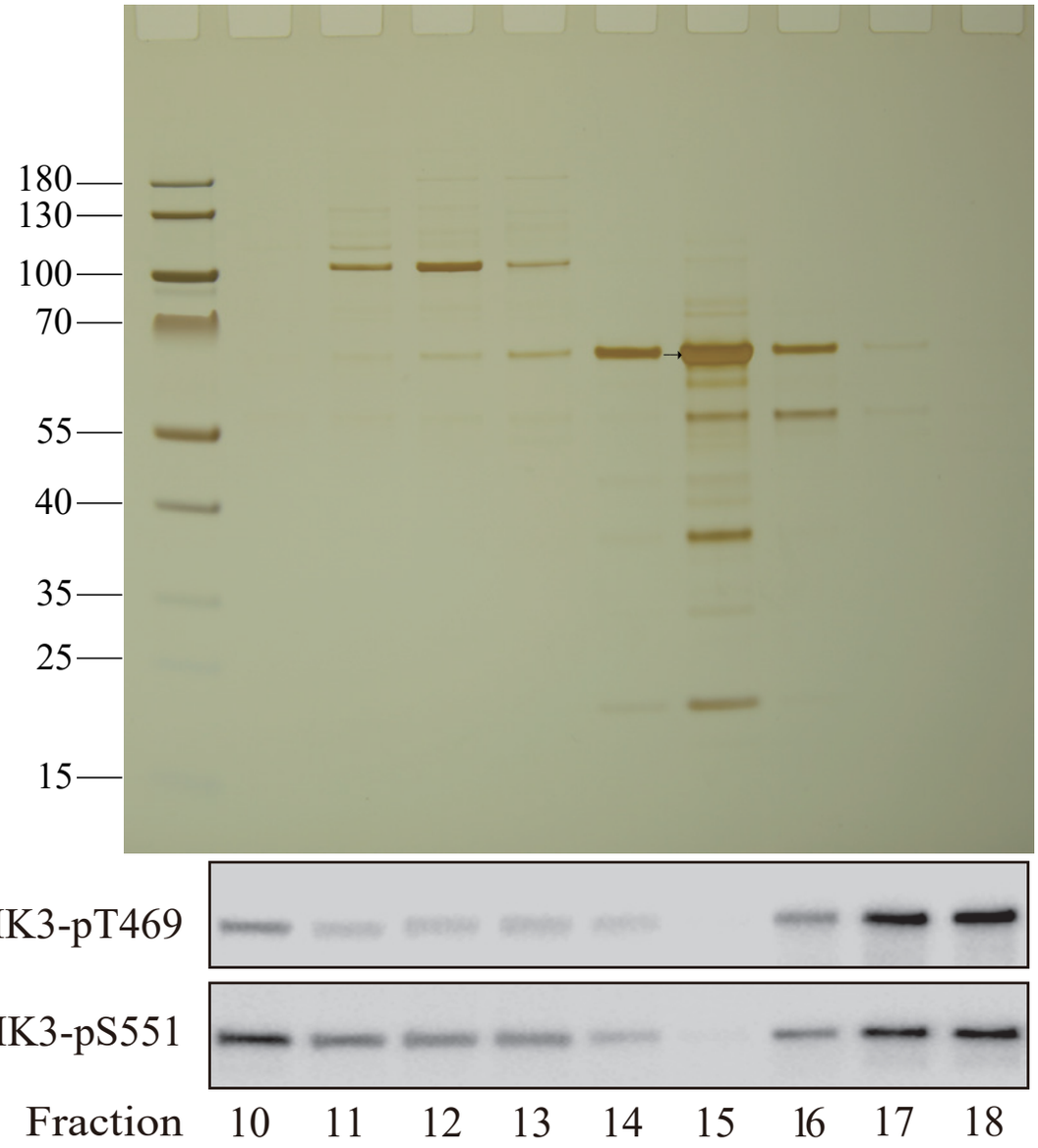

C

Protein	Mascot score	AA (amino acid)	MW	Matched peptides
PPP3CA	300.723	521	58688	88
PPP3CB	84.620	524	59024	30
PPP3CC	23.393	512	58129	16
PPP5C	4.287	499	56879	9

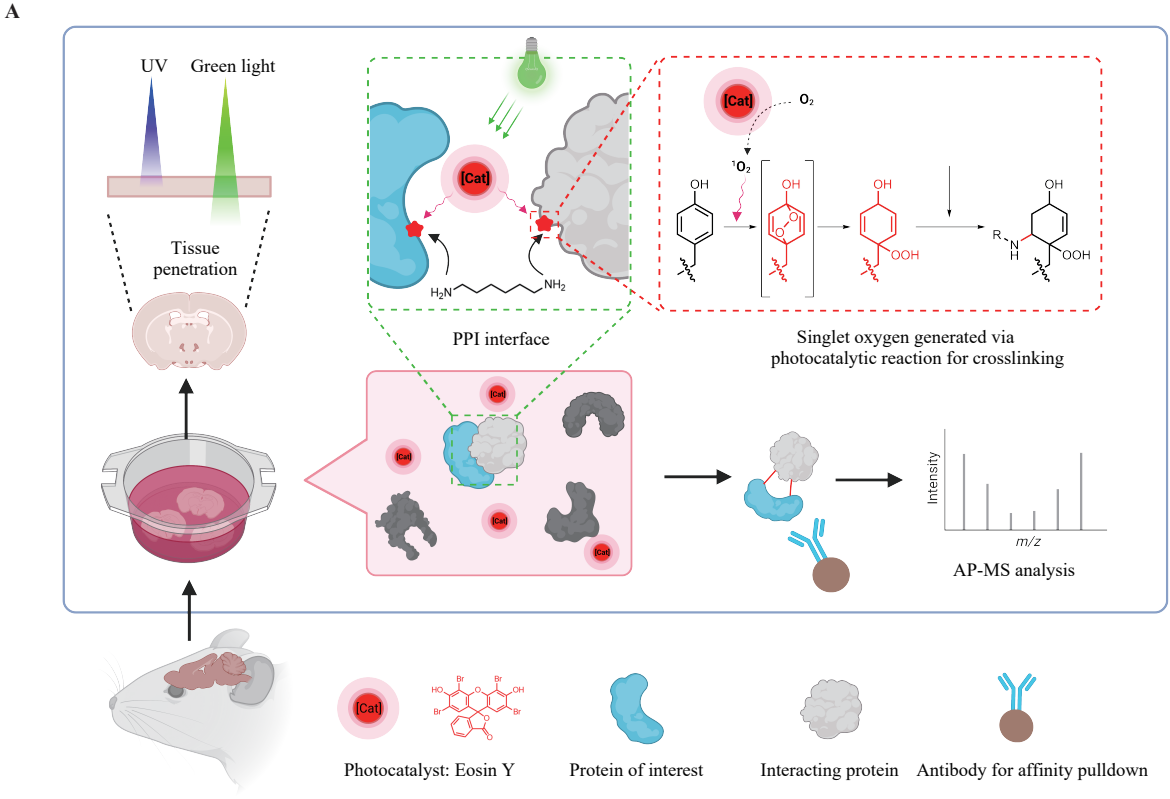
A
UV
Green light
Tissue penetration
[Cat]
PPI interface
Singlet oxygen generated via photocatalytic reaction for crosslinking
AP-MS analysis
Intensity
m/z
Photocatalyst: Eosin Y
Protein of interest
Interacting protein
Antibody for affinity pulldown

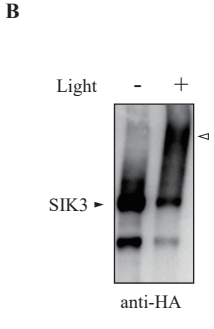
B
Light
-
+
SIK3
anti-HA

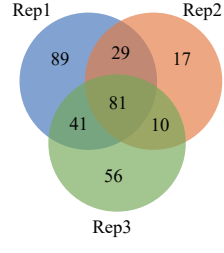
C
Rep1
Rep2
Rep3
89
29
17
81
41
10
56

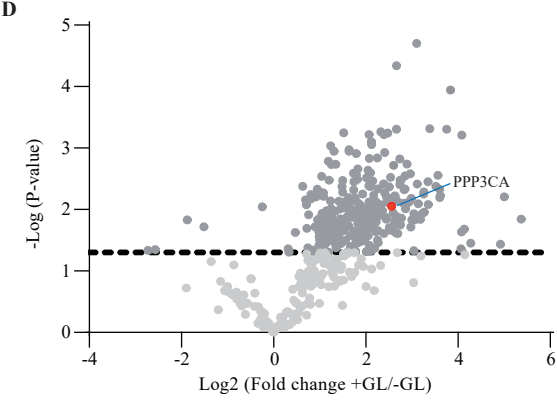
D
-Log (P-value)
Log2 (Fold change +GL/-GL)
PPP3CA

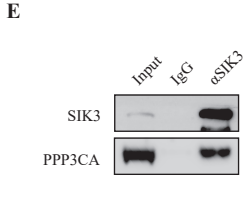
E
Input
IgG
αSIK3
SIK3
PPP3CA

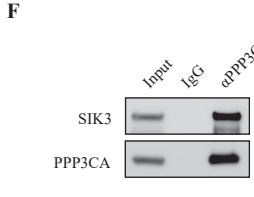
F
Input
IgG
αPPP3CA
SIK3
PPP3CA

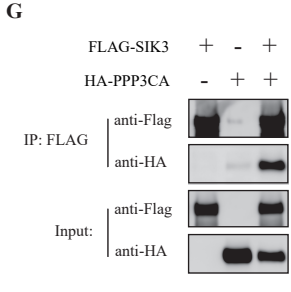
G
FLAG-SIK3
HA-PPP3CA
IP: FLAG
anti-Flag
anti-HA
Input:
anti-Flag
anti-HA

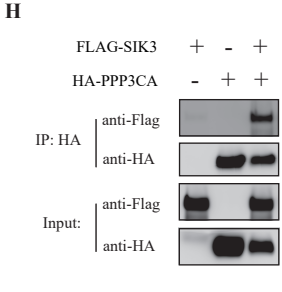
H
FLAG-SIK3
HA-PPP3CA
IP: HA
anti-Flag
anti-HA
Input:
anti-Flag
anti-HA

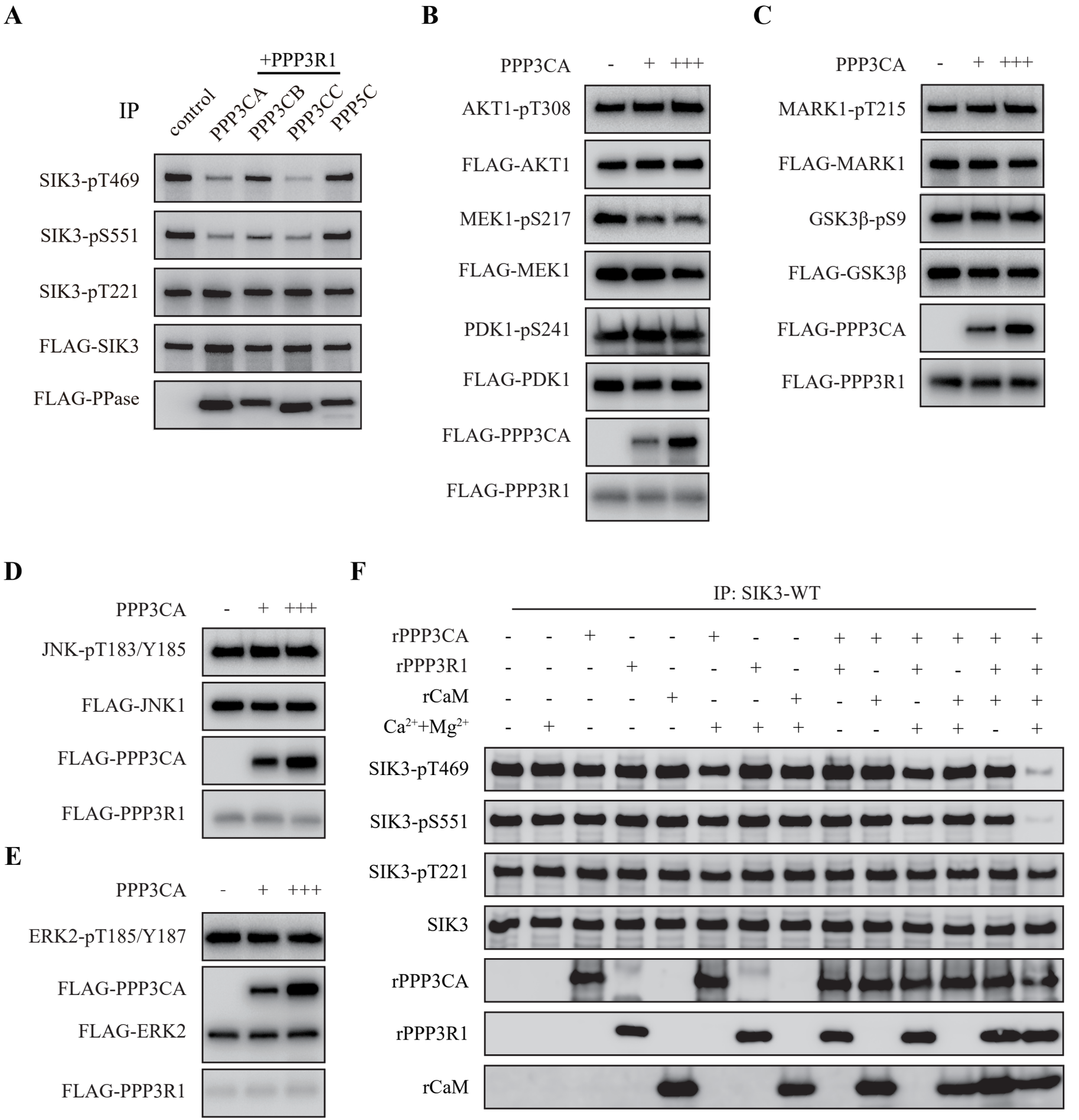
A
+PPP3R1
IP
control
PPP3CA
PPP3CB
PPP3CC
PPP5C
SIK3-pT469
SIK3-pS551
SIK3-pT221
FLAG-SIK3
FLAG-PPase
B
PPP3CA - + +++
AKT1-pT308
FLAG-AKT1
MEK1-pS217
FLAG-MEK1
PDK1-pS241
FLAG-PDK1
FLAG-PPP3CA
FLAG-PPP3R1
C
PPP3CA - + +++
MARK1-pT215
FLAG-MARK1
GSK3β-pS9
FLAG-GSK3β
FLAG-PPP3CA
FLAG-PPP3R1
D
PPP3CA - + +++
JNK-pT183/Y185
FLAG-JNK1
FLAG-PPP3CA
FLAG-PPP3R1
E
PPP3CA - + +++
ERK2-pT185/Y187
FLAG-PPP3CA
FLAG-ERK2
FLAG-PPP3R1
F
IP: SIK3-WT
rPPP3CA
rPPP3R1
rCaM
Ca2+ +Mg2+
SIK3-pT469
SIK3-pS551
SIK3-pT221
SIK3
rPPP3CA
rPPP3R1
rCaM

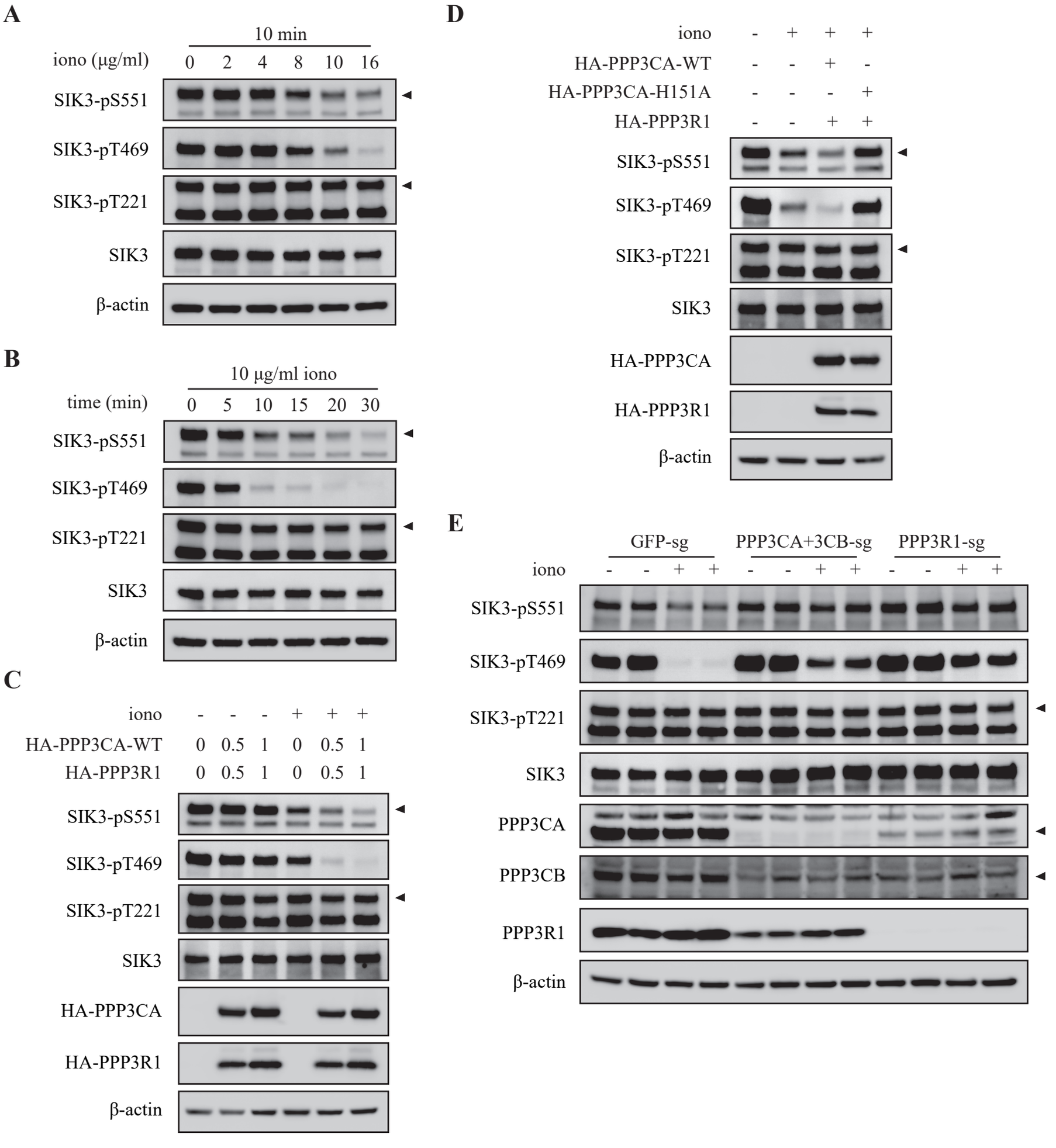
A
10 min
iono (μg/ml)
0 2 4 8 10 16
SIK3-pS551
SIK3-pT469
SIK3-pT221
SIK3
β-actin
B
10 μg/ml iono
time (min)
0 5 10 15 20 30
SIK3-pS551
SIK3-pT469
SIK3-pT221
SIK3
β-actin
C
iono - - - + + +
HA-PPP3CA-WT 0 0.5 1 0 0.5 1
HA-PPP3R1 0 0.5 1 0 0.5 1
SIK3-pS551
SIK3-pT469
SIK3-pT221
SIK3
HA-PPP3CA
HA-PPP3R1
β-actin
D
iono - + + +
HA-PPP3CA-WT - - + -
HA-PPP3CA-H151A - - - +
HA-PPP3R1 - - + +
SIK3-pS551
SIK3-pT469
SIK3-pT221
SIK3
HA-PPP3CA
HA-PPP3R1
β-actin
E
GFP-sg
PPP3CA+3CB-sg
PPP3R1-sg
iono - - + + - - + + - - + +
SIK3-pS551
SIK3-pT469
SIK3-pT221
SIK3
PPP3CA
PPP3CB
PPP3R1
β-actin

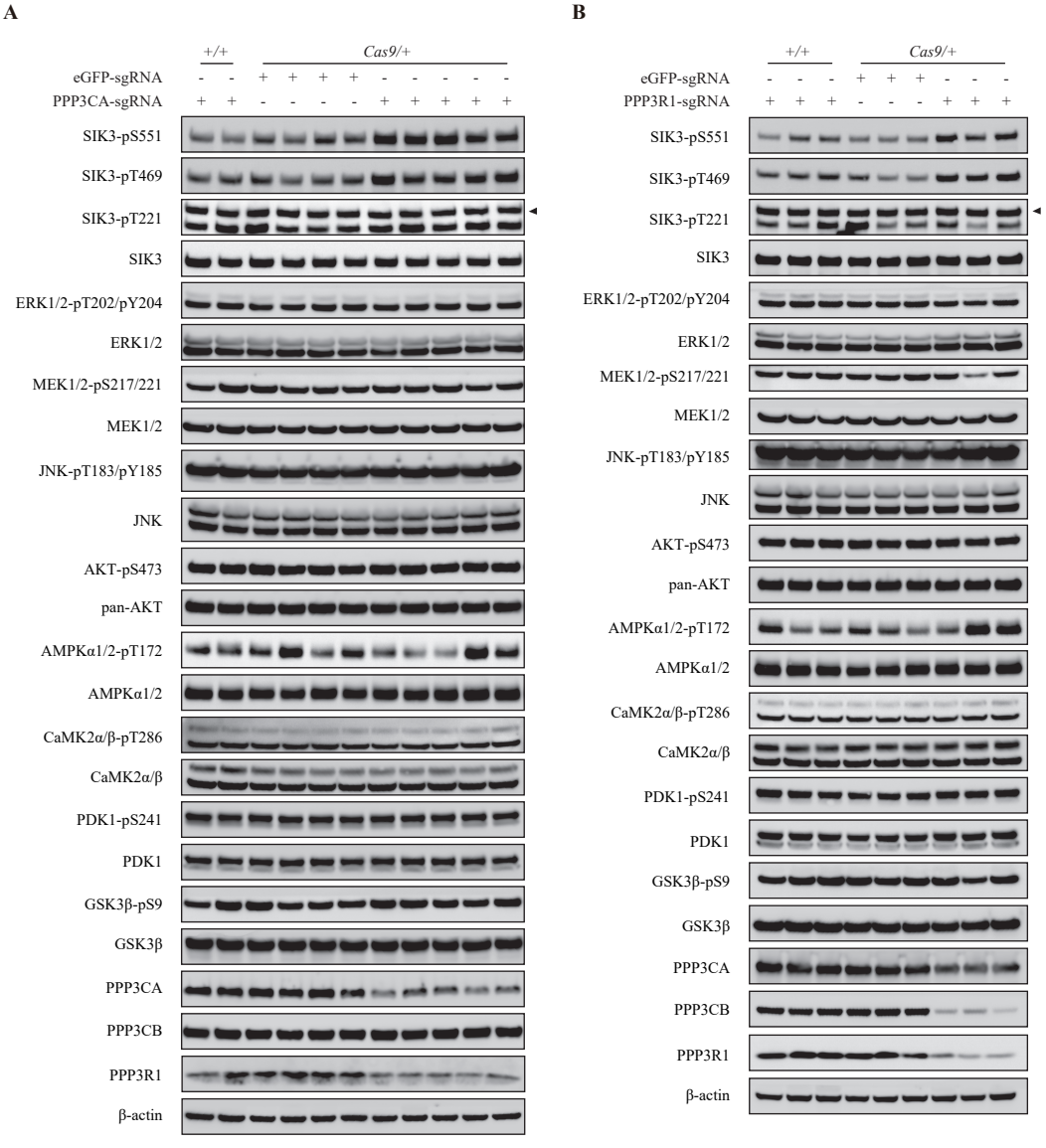
A
+/+
Cas9/+
eGFP-sgRNA
PPP3CA-sgRNA
SIK3-pS551
SIK3-pT469
SIK3-pT221
SIK3
ERK1/2-pT202/pY204
ERK1/2
MEK1/2-pS217/221
MEK1/2
JNK-pT183/pY185
JNK
AKT-pS473
pan-AKT
AMPKα1/2-pT172
AMPKα1/2
CaMK2α/β-pT286
CaMK2α/β
PDK1-pS241
PDK1
GSK3β-pS9
GSK3β
PPP3CA
PPP3CB
PPP3R1
β-actin
B
+/+
Cas9/+
eGFP-sgRNA
PPP3R1-sgRNA
SIK3-pS551
SIK3-pT469
SIK3-pT221
SIK3
ERK1/2-pT202/pY204
ERK1/2
MEK1/2-pS217/221
MEK1/2
JNK-pT183/pY185
JNK
AKT-pS473
pan-AKT
AMPKα1/2-pT172
AMPKα1/2
CaMK2α/β-pT286
CaMK2α/β
PDK1-pS241
PDK1
GSK3β-pS9
GSK3β
PPP3CA
PPP3CB
PPP3R1
β-actin

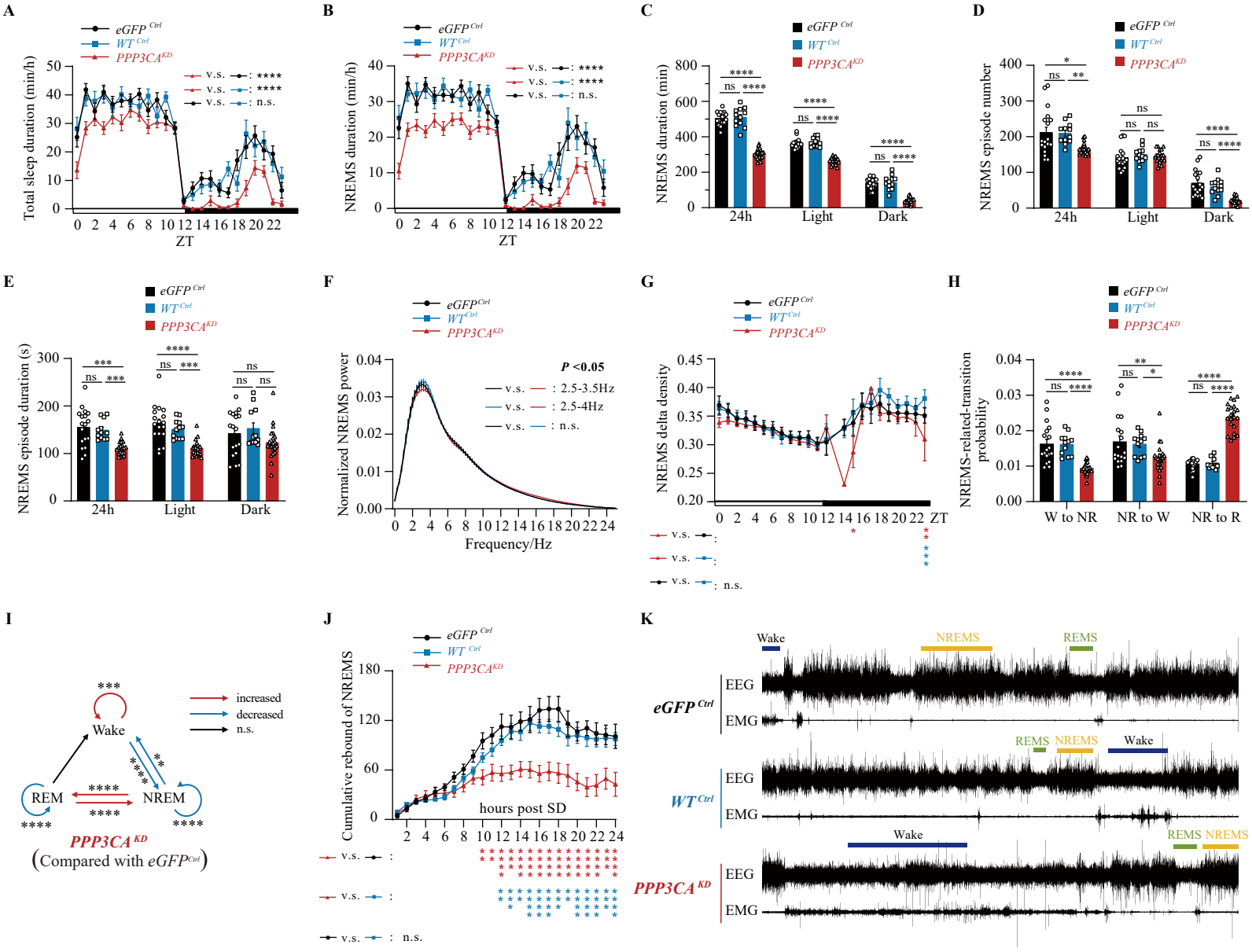
A
B
C
D
E
F
G
H
I
J
K
eGFP Ctrl
WT Ctrl
PPP3CA KD
Total sleep duration (min/h)
NREMS duration (min/h)
NREMS duration (min)
NREMS episode number
NREMS episode duration (s)
Normalized NREMS power
NREMS delta density
NREMS-related-transition probability
Cumulative rebound of NREMS
ZT
Frequency/Hz
hours post SD
24h
Light
Dark
W to NR
NR to W
NR to R
P <0.05
v.s. : 2.5-3.5Hz
v.s. : 2.5-4Hz
v.s. : n.s.
increased
decreased
n.s.
Wake
REM
NREM
PPP3CA KD
(Compared with eGFP Ctrl)
EEG
EMG
NREMS
REMS

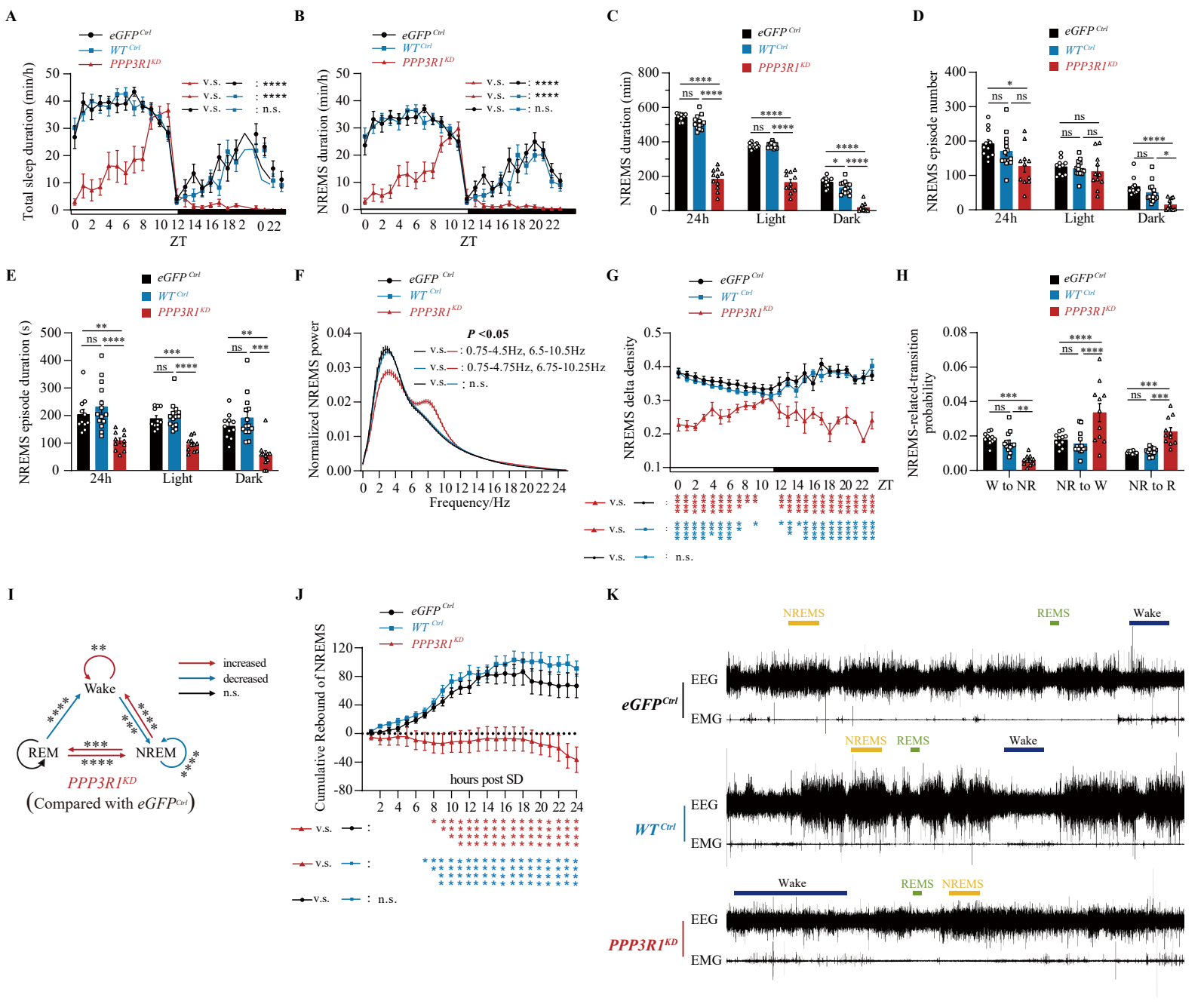
A
B
C
D
E
F
G
H
I
J
K
eGFP Ctrl
WT Ctrl
PPP3R1 KD
Total sleep duration (min/h)
NREMS duration (min/h)
NREMS duration (min)
NREMS episode number
NREMS episode duration (s)
Normalized NREMS power
NREMS delta density
NREMS-related-transition probability
Cumulative Rebound of NREMS
ZT
Frequency/Hz
hours post SD
24h
Light
Dark
W to NR
NR to W
NR to R
P <0.05
v.s. : 0.75-4.5Hz, 6.5-10.5Hz
v.s. : 0.75-4.75Hz, 6.75-10.25Hz
v.s. : n.s.
v.s. : ****
v.s. : n.s.
increased
decreased
n.s.
Wake
REM
NREM
PPP3R1 KD
(Compared with eGFP Ctrl)
NREMS
REMS
EEG
EMG